Research Square

Preprints are preliminary reports that have not undergone peer review.
They should not be considered conclusive, used to inform clinical practice,
or referenced by the media as validated information.

Targeting PCBP1 Sequentially Represses BAG1 and SOX2/β-catenin Axis to Inhibit HCC Cells Proliferation and Reverse Intrinsic Sorafenib Resistance

Zhe Li
The First Affiliated Hospital, Sun Yat-sen University
Jing Yang
Sun Yat-sen University
Chunlong Huang
The First Affiliated Hospital, Sun Yat-sen University
Junxiu Huang
Sun Yat-sen University
Ying Fang
Sun Yat-sen University
Huidan Qiu
Sun Yat-sen University
Zhenyu Hu
Sixth Affiliated Hospital of Sun Yat-sen University
Qiuxia Chen
The First Affiliated Hospital, Sun Yat-sen University
Guang Lu
Sun Yat-sen University
Zifeng Zhang
Xizang Minzu University
Yidi Zhao
Sun Yat-sen University
Banglao Xu
Guangzhou First People's Hospital
Shulan Yang
The First Affiliated Hospital, Sun Yat-sen University
Haihe Wang
wanghaih@mail.sysu.edu.cn

Sun Yat-sen University

Research Article

Keywords: HCC, PCBP1, Sorafenib, Intrinsic resistance, BAG1, SOX2

Posted Date: August 12th, 2026

DOI: https://doi.org/10.21203/rs.3.rs-10654693/v1

License: This work is licensed under a Creative Commons Attribution 4.0 International License.
Read Full License

Additional Declarations: No competing interests reported.

Targeting PCBP1 Sequentially Represses BAG1 and SOX2/β-catenin Axis to Inhibit HCC Cells Proliferation and Reverse Intrinsic Sorafenib Resistance

Zhe Li[1,2,3*], Jing Yang[2*], Chunlong Huang[4*], Junxiu Huang[2], Ying Fang[2], Huidan Qiu[2], Zhenyu Hu[5], Qiuxia Chen[6], Guang Lu[7], Zifeng Zhang[8], Yidi Zhao[2], Banglao Xu[3*], Shulan Yang[1*], Haihe Wang[2,8*]

[1]Centre for Translational Medicine, The First Affiliated Hospital, Sun Yat-sen University, Guangzhou, Guangdong, 510080, China

[2]Department of Biochemistry, Zhongshan School of Medicine, Sun Yat-sen University, Guangzhou, Guangdong, 510080, China

[3]Department of Laboratory Medicine, Guangzhou First People's Hospital, Guangzhou, Guangdong, 510180, China

[4]Department of Hepatobiliary Surgery, The First Affiliated Hospital, Sun Yat-sen University, Guangzhou, Guangdong, 510080, China

[5]Department of Thoracic Surgery, The Sixth Affiliated Hospital, Sun Yat-sen University, Guangzhou, 510655, China.

[6]Department of Traditional Chinese Medicine, The First Affiliated Hospital, Sun Yat-sen University, Guangzhou, Guangdong, 510080, China

[7]Department of Physiology, Zhongshan School of Medicine, Sun Yat-sen University, Guangzhou, Guangdong, 510080, China

[8]Clinical Medical Research Centre for Plateau Gastroenterological Diseases of Xizang Autonomous Region, Xizang Minzu University, Xianyang, 702082, China.

*These authors contributed equally to this work.

Corresponding Authors: Banglao Xu, 1 Panfu Road, Guangzhou, 510180, China, Telephone: +86-20-81048084, E-mail: eyxubl@scut.edu.cn; Shulan Yang, 58 Second Zhongshan Road, Guangzhou, 510080, China, Telephone: +86-20-28823350, E-mail: yangshl3@mail.sysu.edu.cn; Lead contact: Haihe Wang, 74 Second Zhongshan Road, Guangzhou, 510080, China, Telephone: +86-20-87335035, E-mail: wanghaih@mail.sysu.edu.cn.

Abstract

Background: Hepatocellular carcinoma (HCC) ranks as the third leading cause of cancer-related mortality, and sorafenib remains the first-line systemic therapy for advanced HCC. Nevertheless, up to 70% of patients exhibit intrinsic sorafenib resistance with unclear molecular mechanisms.

Methods: In vitro cellular phenotypes including sorafenib sensitivity, proliferation, migration and invasion were assessed via functional experiments. Western blotting, RT-qPCR, RNA immunoprecipitation, immunocytochemistry and RNA-seq analyses were employed to verify the regulatory effect of PCBP1 on BAG1 and the SOX2/β-catenin signaling pathway, as well as to elucidate the mechanism underlying the compensatory restoration of BAG1-p36. In vivo xenograft models were constructed in nude mice to further validate the modulatory role of PCBP1 in sorafenib therapeutic responsiveness, and western blotting was performed to detect the expression of PCBP1, BAG1 and

SOX2 in HCC tissues from drug-resistant and non-resistant patients.

Results: *PCBP1* is significantly upregulated in sorafenib-tolerant HCC tissues and linked to poor prognosis. Physiologically, PCBP1 confers sorafenib resistance, characterized by enhanced sorafenib-induced apoptosis rather than ferroptosis upon transient or stable PCBP1 downregulation in HCC cells. Mechanistically, PCBP1 knockdown induces immediate BAG1-p36 decrease and persistent SOX2 downregulation to promote dramatic sensitivity of HCC cells to sorafenib. Upon sustained PCBP1 knockdown, decreased BAG1-p36 expression recovers over time via compensatory PTBP1 upregulation, but cells retain partial sorafenib sensitivity. Further investigation reveals that persistent suppression of SOX2/β-catenin signaling is attributed to impaired *SOX2* mRNA stability and translation following PCBP1 depletion, which weakens HCC stemness. Co-targeting BAG1 and SOX2 synergistically sustains low BAG1-p36 levels and promotes sorafenib sensitivity. Likewise, PCBP1 depletion effectively inhibits HCC cell proliferation, metastasis and xenograft tumor growth, along with the elevated therapeutic efficacy of sorafenib. Finally, we verified high expression of PCBP1, SOX2 and BAG1 in HCC tissues from patients with post-treatment recurrence.

Conclusions: Our findings unveil PCBP1 as an intrinsic culprit for sorafenib resistance in HCC, and BAG1-p36 adaptive recovery renders acquired resistance. Thus, dual targeting of PCBP1/SOX2 axis and BAG1 would be an impressive strategy to overcome the intrinsic and delay the acquired sorafenib resistance in HCC.

Keywords: HCC, PCBP1, Sorafenib, Intrinsic resistance, BAG1, SOX2

Background

Hepatocellular carcinoma (HCC) accounts for 75%-85% of primary liver cancers, with over 800 000 annual deaths worldwide(Bray et al. 2024, Petrick et al. 2020). As the most common subtype of liver cancer, HCC is often diagnosed at advanced stages due to its asymptomatic early progression, and systemic therapy remains the last resort. Sorafenib, a multi-targeting tyrosine kinase inhibitor, has been the first-line targeted therapy for advanced HCC due to its anti-angiogenesis effects by repressing vascular endothelial growth factor receptor (VEGFR) 2 or platelet-derived growth factor receptor (PDGFR) -β, and triggering cell death by blocking the Ras/Raf/MEK/ERK pathway and system Xc^--mediated ferroptosis(Tang et al. 2020, Li et al. 2023). Moreover, sorafenib also has an autophagic effect in HCC cells(Prieto-Dominguez et al. 2016). However, only 30% patients achieve a clinical response to sorafenib, and up to 70% exhibit intrinsic resistance. Responders still develop acquired resistance within 6 months, resulting in a median 10-11 months of overall survival(Tang et al. 2020). Hitherto, the mechanisms underlying intrinsic sorafenib resistance remain elusive.

Poly(rC)-binding protein 1 (PCBP1) is an evolutionarily conserved RNA/DNA-binding protein with three KH domains for its specific binding to cytosine-rich regions in nucleic acids(Zhang et al. 2020). Functionally, PCBP1 participates in multiple post-transcriptional processes, including alternative splicing, mRNA stability, and cap-independent translation to modulate hypoxia, autophagy, apoptosis, or ferroptosis for cell survival, proliferation, or cell death(Bradley et al. 2023, Tan et al. 2024, Yang et al.

2023, Nandal et al. 2011, Zhang et al. 2016, Ansa-Addo et al. 2020, Ishii et al. 2018). However, the role of PCBP1 is context-dependent in cancers. For instance, in prostate and pancreatic cancer, PCBP1 acts as a tumor suppressor by inhibiting MAPK signaling or alternative splicing of integrin-β1(Zhang et al. 2018, Jiang et al. 2017), but in head and neck cancer, it promotes ferroptosis resistance by repressing ferritinophagy(Lee et al. 2022). Notably, PCBP1 has been implicated in liver physiology, as hepatocyte-specific PCBP1 knockout disrupts iron homeostasis, leading to hepatic steatosis and inflammation in mice(Protchenko et al. 2021). However, its expression and physiological role in HCC and therapy efficacy are mysterious. We tentatively analyzed the Gene Expression Omnibus (GEO) database of HCC and revealed that PCBP1 is markedly upregulated in sorafenib-insensitive HCC tissues, indicating PCBP1 as a key mediator of intrinsic sorafenib resistance.

Bcl-2–associated athanogene-1 (BAG1), a member of the BAG family, has four isoforms, BAG1-L/p50, BAG1-M/p46, BAG1-S/p36, BAG1-p29, produced by alternative translation initiation with distinct expression patterns and functional roles in different tumor types(Mariotto et al. 2020). High BAG1 expression correlates with favorable prognosis in breast cancer, clear cell renal cell carcinoma, and non-small cell lung cancer(Papadakis et al. 2017, Wu et al. 2021, Rorke et al. 2001), but with poor outcomes in lung adenocarcinoma, colorectal cancer, melanoma and HCC(Fan et al. 2021, Bai et al. 2007, D'Arcangelo et al. 2018, Ni et al. 2013). In several cancer cell lines, BAG1 overexpression enhances anti-apoptotic activity and drug resistance via interacting with Bcl-2 and HSP70 to promote chemoresistance(Kudoh et al. 2002,

Townsend et al. 2003, Kizilboga et al. 2019, Liu et al. 2017, Mariotto et al. 2021). PCBP1 and Polypyrimidine tract-binding protein 1 (PTBP1) binds the internal ribosome entry site (IRES) of *BAG1* mRNA to enhance its translation activity in certain cell lines(Pickering et al. 2003). However, whether this interaction occurs and regulates sorafenib sensitivity in HCC remains unknown.

We further noted a master regulator of embryonic and induced pluripotent stem cells, Sex-determining region Y-box 2 (SOX2), changes with PCBP1 expression level. SOX2 is a core transcription factor for cancer stem cell (CSC) characteristics, epithelial-mesenchymal transition (EMT) and drug resistance in multiple cancers, including HCC(Novak et al. 2020, Mirzaei et al. 2022, Huser et al. 2018, Liu et al. 2022). In colorectal and prostate cancers, SOX2 exerts its effects through activation of the Wnt/β-catenin pathway, a highly conserved signaling cascade frequently dysregulated in HCC(Tang et al. 2018, Zhu et al. 2021, Song et al. 2024), but whether SOX2 regulates Wnt/β-catenin in HCC remains unknown. Aberrant β-catenin activation drives uncontrolled cell proliferation and inhibits apoptosis, and it is linked to sorafenib resistance in preclinical models(Zhao et al. 2024, Leung et al. 2021), but the upstream regulators of SOX2 in HCC have not been identified.

Here, we demonstrated the clinical correlation between PCBP1 expression and tumor progression, sorafenib sensitivity or prognosis in HCC, and unveiled the molecular mechanisms underlying sorafenib response by silencing PCBP1. Thus, a combinatorial therapeutic strategy would be of help to overcome the intrinsic and delay the acquired sorafenib resistance.

Methods

Cell Lines and Authentication

Cell lines: Hep3B, Snu449, and 293T cells were purchased from the American Type Culture Collection (ATCC, Manassas, USA). Huh7 and LM3 cells were kindly provided by Prof. Shijun Zhang (The First Affiliated Hospital of Sun Yat-sen University, Guangzhou, China). All cell lines were authenticated by short tandem repeat (STR) profiling (Jennio Biological Technology, Guangzhou, China) within 6 months of experimentation, and tested negative for mycoplasma using the MycoAlert™ Mycoplasma Detection Kit (LT07-318, Lonza, Basel, Switzerland). Cells were maintained in Dulbecco's Modified Eagle Medium (DMEM; C11995500BT, Gibco, USA) supplemented with 10% fetal bovine serum (FBS; F7524, Sigma-Aldrich, USA) and 100 U/mL penicillin/50 μg/mL streptomycin (SV30010, HyClone, USA) at 37°C in a humidified atmosphere with 5% CO_2.

Reagents and Antibodies

Sorafenib (S7397), RSL3 (S8155, ferroptosis inducer), XAV-939 (S1180, Wnt/β-catenin inhibitor) were purchased from Selleck Chemicals (Houston, USA). Ferrostatin-1 (Fer-1; HY-100579, ferroptosis inhibitor), Z-VAD-FMK (HY-16658B, pan-caspase inhibitor), MG132 (HY-13259, proteasome inhibitor), cycloheximide (CHX; HY-12320, translation inhibitor), and actinomycin D (ACTD; HY-17559, transcription inhibitor) were purchased from MCE (New Jersey, USA). MK-2206 (A145592, Akt inhibitor) was purchased from Ambeed (USA). Cell Counting Kit-8

(CCK-8; HY-K0301) was from MCE; Annexin V-FITC/PI Apoptosis Detection Kit (BB-4101) was from Bestbio (Shanghai, China); PureBinding® RNA Immunoprecipitation (RIP) Kit (P0101) was from GENESEED (Guangzhou, China); Lipofectamine™ 3000 (L3000075) and TRIzol™ Reagent (15596018CN) was from Thermo Fisher Scientific (Waltham, USA); StarScript III All-in-one RT Mix with gDNA Remover (A230) and 2×RealStar Fast SYBR qPCR Mix (A301) were from GenStar (Beijing, China). Primary antibodies and secondary antibodies are listed in Supplementary Table S1, including catalog numbers, manufacturers, and dilution ratios for Western blot (WB) and immunocytochemistry (ICC).

Animals and Ethical Approval

Four-week-old male BALB/c nude mice (specific pathogen-free grade) were purchased from the Laboratory Animal Center of Sun Yat-sen University (Guangzhou, China). Mice were housed in a temperature-controlled (22±2°C) and light-cycled (12 h light/12 h dark) environment with free access to food and water. All animal experiments were approved by the Institutional Animal Care and Use Committee (IACUC) of Sun Yat-sen University (approval number: SYSU-IACUC-2024-002633) and conducted in accordance with the Guide for the Care and Use of Laboratory Animals (National Institutes of Health, USA).

Transient siRNA transfection

Small interfering RNAs (siRNAs) targeting PCBP1, BAG1, PTBP1 and SOX2 (sequences in Supplementary Table S2) were synthesized by Tsingke Biotechnology (Beijing, China). Cells transfected with 50 nM siRNA using Lipofectamine™ 3000

according to the manufacturer's protocol.

Stable cell line establishment

For stable knockdown of PCBP1, BAG1 and SOX2, short hairpin RNAs (shRNAs, sequences in Supplementary Table S2) were cloned into the pLKO.1 lentiviral vector. For lentivirus packaging, 293T cells were co-transfected with pLKO.1-shRNA, psPAX2 (packaging plasmid), and pCMV-VSV-G (envelope plasmid) using Lipofectamine™ 3000. Viral supernatants were collected 48-72 h post-transfection, filtered through a 0.45 μm membrane, and used to infect HCC cells. Stable cell lines were selected with 2 μg/mL puromycin (P9620, Sigma-Aldrich) for 2 weeks, and knockdown efficiency was verified. For the stable and transient overexpressing cell lines, full-length cDNAs of PCBP1, BAG1-p36, PTBP1 and SOX2 were cloned into the pCDH-CMV-MCS-EF1-Neo or pCMV-Tag2B vector. Cells were transfected with 2 μg plasmid using Lipofectamine™ 3000 and the overexpression efficiency was confirmed at 48 h post-transfection. shRNAs and primers were synthesized by GENEWIZ (Suzhou, China).

CCK-8 assay

Cells were seeded in 96-well plates at a density of 5×10^3 cells/well and cultured overnight. Cells were then treated with sorafenib at concentrations ranging from 0 to 20 μM for 24 or 48 h. Ten microliters of CCK-8 reagent was added to each well, and the plates were incubated at 37°C for 2 h. Absorbance at 450 nm was measured using a Tecan Infinite M200 microplate reader (Männedorf, Switzerland). Cell viability was calculated relative to the control group (0 μM sorafenib), and the half-maximal

inhibitory concentration (IC_{50}) was determined using GraphPad Prism 8 software (La Jolla, USA).

Flow cytometry for cell death

Cells were seeded in 6-well plates and treated with sorafenib (10 μM; 36 h for Huh7 and 48 h for Hep3B). Cells were harvested by trypsinization, washed twice with cold phosphate-buffered saline (PBS), and stained with propidium iodide (PI) or Annexin V-FITC/PI using the Annexin V-FITC/PI Apoptosis Detection Kit. Stained cells were analyzed using a CytoFLEX S flow cytometer (Beckman Coulter, Brea, USA), and data were processed with CytExpert software (Beckman Coulter). Cell death was defined as the percentage of Annexin V^+/PI^- (early apoptosis) and Annexin V^+/PI^+ (late apoptosis/necrosis) cells.

Colony formation assay

Cells were seeded in 6-well plates at a density of 700 cells/well and cultured for 14 days. Colonies were fixed with 4% paraformaldehyde (BL539A, Biosharp, Hefei, China) for 15 min at room temperature, stained with 0.5% crystal violet (C0121, Beyotime, Shanghai, China) for 30 min, and washed with PBS. Colonies containing > 50 cells were counted using ImageJ software (National Institutes of Health, USA).

Wound healing assay

Cells were seeded in 6-well plates with two-well silicone inserts (16211, LABSELECT, Shanghai, China) and cultured until confluent. The inserts were removed to create a uniform scratch, and cells were washed with PBS to remove detached cells. Cells were then cultured in serum-free DMEM, and images were captured at 0 and 72 h using an

Olympus IX73 inverted microscope (Tokyo, Japan). The scratch closure rate was calculated as (initial scratch width - final scratch width)/initial scratch width × 100%.

Transwell migration and invasion assays

Transwell chambers (353097, Corning, USA) were placed in 24-well plates. For invasion assays, the upper chamber membrane was coated with Matrigel (356234, Corning) diluted 1:8 with serum-free DMEM and incubated at 37°C for 30 min to solidify. Cells were resuspended in serum-free DMEM at a density of 1×10^5 cells/mL, and 200 μL of cell suspension was added to the upper chamber. 500 μL of DMEM supplemented with 20% FBS was added to the lower chamber as a chemoattractant. After incubation for 24 h (migration) or 48 h (invasion), non-migrated/non-invaded cells on the upper surface of the membrane were removed with a cotton swab. Migrated/invaded cells on the lower surface were fixed with 4% paraformaldehyde, stained with 0.5% crystal violet, and counted under a microscope (5 random fields per chamber).

Western blot (WB)

Cells and tissues were harvested and lysed in RIPA lysis buffer (P0013B, Beyotime) supplemented with 1% phenylmethylsulfonyl fluoride (PMSF; ST506, Beyotime) and 1% phosphatase inhibitor cocktail (CW2383S, Cwbio, Taizhou, China) on ice for 30 min. Lysates were centrifuged at 12 000 × g for 15 min at 4°C, and the supernatant was collected. Protein concentration was determined using the BCA Protein Assay Kit (27337, Thermo Fisher Scientific). 20 μg of protein per sample was separated by 10%-12% sodium dodecyl sulfate-polyacrylamide gel electrophoresis (SDS-PAGE) and

transferred to polyvinylidene difluoride (PVDF) membranes (03010040001, Millipore, Billerica, USA). Membranes were blocked with 5% non-fat milk in Tris-buffered saline with Tween-20 (TBST) for 1 h at room temperature, then incubated with primary antibodies overnight at 4°C. After washing with TBST, membranes were incubated with horseradish peroxidase (HRP)-conjugated secondary antibodies for 1 h at room temperature. Protein bands were visualized using an enhanced chemiluminescence (ECL) detection system (WBKLS0500, Millipore) and imaged with a ChemiDoc™ Touch imaging system (Bio-Rad, Hercules, USA). Band intensity was quantified using ImageJ software, with β-Actin as the loading control.

Real-time quantitative PCR (RT-qPCR)

Total RNA was extracted from cells using TRIzol™ Reagent according to the manufacturer's protocol. RNA concentration and purity were measured using a NanoDrop One spectrophotometer (Thermo Fisher Scientific). 1 μg of total RNA was reverse-transcribed into complementary DNA (cDNA) using the StarScript III All-in-one RT Mix with gDNA Remover to eliminate genomic DNA contamination. RT-qPCR was performed using the 2×RealStar Fast SYBR qPCR Mix on a CFX Opus 96 Real-Time PCR System (Bio-rad). The cycling conditions were: 95°C for 2 min, followed by 40 cycles of 95°C for 15 s and 60°C for 30 s. GAPDH or β-Actin was used as the internal reference gene, and relative gene expression was calculated using the $2^{-\Delta\Delta Ct}$ method. Primer sequences are listed in Supplementary Table S3.

RNA Immunoprecipitation (RIP)

RIP assays were performed using the PureBinding® RIP Kit according to the

manufacturer's instructions. Briefly, 1×10^7 cells were lysed in 1 mL of lysis buffer, then 50 µl and 100 µl of supernatants were reserved for protein and RNA input controls. The remaining lysate was incubated with Protein A+G agarose beads conjugated to anti-PCBP1 antibody or normal rabbit IgG (negative control) overnight at 4°C with rotation (10 rpm). Beads were washed five times with wash buffer, and bound RNA was eluted and purified. The enrichment of *BAG1* and *SOX2* mRNA in the immunoprecipitated fraction was detected by RT-qPCR, with input RNA as the reference.

RNA sequencing (RNA-seq)

Total RNA was extracted from stable PCBP1-knockdown and control Hep3B cells using TRIzol™ Reagent. RNA quality was assessed using an Agilent 2100 Bioanalyzer (Agilent Technologies, Santa Clara, USA), and only RNA with an RNA Integrity Number (RIN) > 8.0 was used for library construction. cDNA libraries were prepared using the Illumina® Stranded mRNA Prep Kit (Illumina, San Diego, USA) according to the manufacturer's protocol. Libraries were sequenced on an Illumina NovaSeq 6000 platform (150 bp paired-end reads) by Majorbio Biomedical Technology (Shanghai, China), with ≥ 6 Gb of clean data per sample. Raw reads were filtered to remove adaptor sequences and low-quality reads, then aligned to the human reference genome (hg38) using HISAT2. Differentially expressed genes (DEGs) were identified using DESeq2 with the criteria of false discovery rate (FDR) < 0.05 and absolute fold change (FC) ≥ 2(Love et al. 2014). Gene Ontology (GO) enrichment analysis and Kyoto Encyclopedia of Genes and Genomes (KEGG) pathway analysis were performed using Goatools and KOBAS, respectively, with $P < 0.05$ considered statistically significant(Klopfenstein et

al. 2018, Bu et al. 2021).

Intracellular lipid peroxide detection

Cells were seeded in 6-well plates and treated with sorafenib (10 μM) for 24 h. Cells were incubated with 1 μM Liperfluo (L248, Dojindo) in serum-free DMEM at 37°C for 30 min. After washing with PBS, cells were harvested by trypsinization and resuspended in PBS. Lipid peroxide levels were analyzed using a CytoFLEX S flow cytometer, with fluorescence intensity reflecting ferroptosis activity.

Intracellular Fe^{2+} measurement

Intracellular Fe^{2+} content was detected using the Ferrous Ion Content Assay Kit (BC5415, Solarbio, Beijing, China) according to the manufacturer's instructions. Briefly, 1×10^7 cells were harvested, resuspended in 1 mL of lysate, and sonicated on ice. Lysates were centrifuged at 10 000 × g for 10 min at 4°C, and the supernatant was collected. 200 μL of supernatant was mixed with 100 μL of Reagent I, and the absorbance at 593 nm was measured using a microplate reader. Fe^{2+} concentration was calculated using a standard curve.

Malondialdehyde (MDA) assay

MDA levels (a marker of lipid peroxidation) were measured using the Malondialdehyde Content Assay Kit (BC0025, Solarbio). Cells were treated with sorafenib for 36 h, harvested, and resuspended in 1 mL of lysate. After sonication and centrifugation, the supernatant was mixed with Reagent I+II and Reagent III, then incubated at 100°C for 60 min. Absorbance at 532 nm and 600 nm was measured, and MDA content was calculated using the formula provided by the kit.

Immunocytochemical (ICC) analysis

Cells grown on coverslips were fixed with 4% paraformaldehyde for 15 min and blocked with 3% bovine serum albumin (BSA) in TBST. After permeabilization with 0.1% Triton X-100 (P0096, Beyotime), cells were incubated overnight at 4℃ with primary antibodies diluted in blocking solution. Secondary antibodies in blocking buffer were applied for 2 h at room temperature. The images were captured using a ZEISS LSM 880 with Airyscan (Oberkochen, Germany).

Cell migration assay in zebrafish vivo

Zebrafish embryos (2-3 days post-fertilization) were obtained from the Model Animal Research Center of Sun Yat-sen University. Hep3B cells were stained with 5 μM Dil (C1036, Beyotime) at 37°C for 15 min, washed with PBS, and resuspended in complete medium at a density of 2×10^7 cells/mL. Approximately 200 stained cells were injected into the yolk sac of each zebrafish embryo using a microinjection system (Eppendorf, Hamburg, Germany). Embryos were incubated at 34°C, and cell migration was observed under a fluorescence microscope (Olympus) at 0 and 7 days post-injection. The number of migrated cells and migration distance from the yolk sac were quantified using ImageJ software.

Subcutaneous xenograft model

Five-week-old male BALB/c nude mice were randomly divided into four groups (n=6 per group): (1) Control (Hep3B cells transfected with empty pLKO.1 vector); (2) Control + Sorafenib (control cells + sorafenib treatment); (3) shPCBP1 + Sorafenib (Hep3B cells with stable PCBP1 knockdown + sorafenib treatment); (4) shPCBP1 +

SOX2 + Sorafenib (shPCBP1 cells with stable SOX2 over-expression + sorafenib treatment). For tumor cell inoculation, 5×10^6 cells were resuspended in 0.15 mL of a 1:1 mixture of DMEM and Matrigel (356234, Corning) and subcutaneously injected into the flanks of each mouse. When tumors reached an average volume of ~1 000 mm^3, mice in the sorafenib treatment groups received intraperitoneal injections of sorafenib (30 mg/kg/day), while control groups received an equal volume of vehicle (5% DMSO + 40% PEG300 + 5% Tween-80 + 50% H_2O). Tumor volume was measured every 2 days using a digital caliper and calculated as $V = 0.5 \times length \times width^2$. After 2 weeks of treatment, mice were euthanized by cervical dislocation, and tumors were excised and weighed.

Data Analysis

All experiments were performed at least three times independently. Data are presented as the mean ± standard deviation (SD). Statistical analysis was conducted using GraphPad Prism 8 software and R 4.2.0 software (R Foundation for Statistical Computing, Vienna, Austria). Differences between two groups were analyzed using two-tailed Student's t-tests, while differences among three or more groups were analyzed using one-way analysis of variance (ANOVA) followed by Tukey's post-hoc test. Survival curves were generated using the Kaplan-Meier method and compared using the log-rank test. For RNA-seq data, DEG analysis was performed using DESeq2, and GO/KEGG enrichment analyses were performed with $P < 0.05$ considered statistically significant. A P value < 0.05 was defined as statistically significant for all other assays.

Results

PCBP1 is upregulated in sorafenib-tolerating HCC patients and correlates with poor prognosis

To explore the possible candidates in sorafenib sensitivity, we first analyzed the RNA-seq data in sorafenib-treated HCC patients using the GEO dataset and showed that *PCBP1* mRNA levels were dramatically higher in sorafenib-insensitive HCC patients than in those sensitive ones (Fig. 1A). Consistently, sorafenib-resistant Hep3B (indicated in GSE248769) and Huh7 cells induced by long-term sorafenib exposure exhibited higher *PCBP1* mRNA expression than their parental counterparts (Fig. 1B). These results suggested that PCBP1 mediates an intrinsic resistance in HCC.

Given that drug sensitivity often correlates with patient prognosis, we analyzed the survival data from The Cancer Genome Atlas (TCGA) HCC cohort. Patients with high PCBP1 expression (best cutoff) had significantly shorter overall survival (OS) with a median of 37.83 vs. 61.73 months (Fig. 1C) and recurrence-free survival (RFS) with a median of 21.23 vs. 36.1 months (Fig. 1D) than those with low PCBP1 expression.

To characterize PCBP1 expression in HCC, we analyzed transcriptomic data from TCGA and proteomic data from the Clinical Proteomic Tumor Analysis Consortium (CPTAC). PCBP1 mRNA and protein levels were higher in HCC tissues than in adjacent non-tumorous tissues (Figs. 1E-G). To validate these, we assessed the PCBP1 protein level in 6 fresh HCC patient tissues, and immunoblot results showed that PCBP1 is higher in tumor tissues than in adjacent ones (Fig. 1H). Furthermore, we

375 measured PCBP1 expression and its correlation with sorafenib sensitivity in four HCC
376 cell lines (Huh7, Hep3B, LM3, Snu449). Results indicated that the higher PCBP1
377 protein level relates to less sorafenib sensitivity, shown as the increased IC_{50} values in
378 both Hep3B and Snu449 cells, in contrast to the sorafenib-sensitive Huh7 and LM3
379 cells (Figs.1 I, J). Collectively, these data demonstrate that PCBP1 is upregulated in
380 sorafenib-insensitive HCC and correlates with poor patient outcomes.

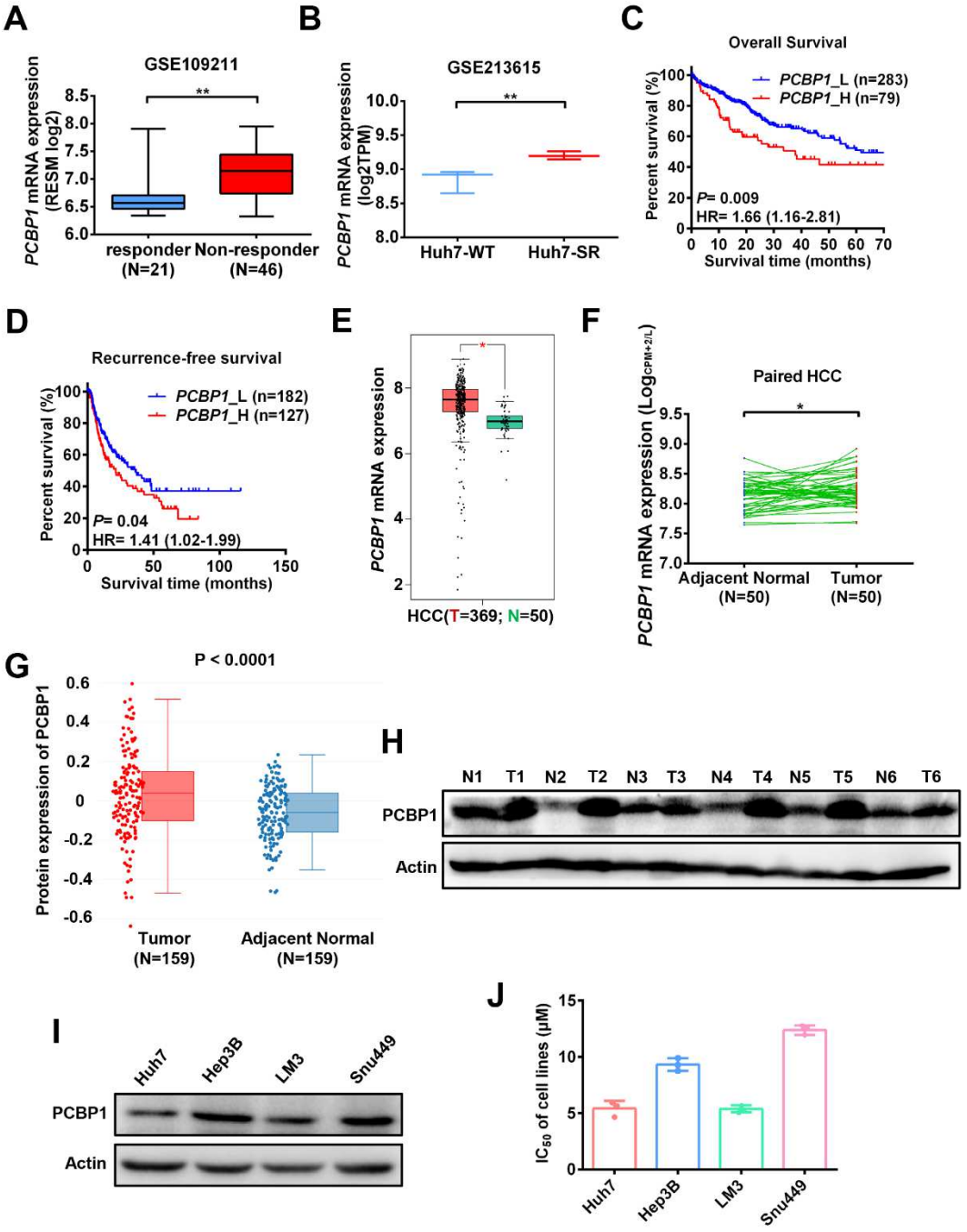


Figure 1

Figure. 1 PCBP1 expression is negatively correlated with sorafenib sensitivity of hepatocellular carcinoma (HCC).

(A) Expression levels of *PCBP1* mRNA in tumor tissues from HCC patients responding

or not responding to sorafenib treatment. **(B)** Expression levels of *PCBP1* mRNA in wild-type and sorafenib-resistant Huh7 cells. **(C, D)** Overall survival (C) and recurrence-free survival (D) of HCC patients with high *PCBP1* mRNA expression based on data of The Cancer Genome Atlas (TCGA). **(E-H)** Expression levels of PCBP1 mRNA (E, F) and protein (G, H) in HCC tissues compared with those in adjacent non-tumorous tissues. mRNA data were obtained from TCGA; protein data from the Clinical Proteomic Tumor Analysis Consortium (CPTAC). **(I)** Expression levels of PCBP1 of four HCC cell lines. **(J)** IC_{50} values of sorafenib treatment (24 h, n = 3) of four HCC cell lines. N represents normal, T represents tumor. $*P < 0.05$, $**P < 0.01$.

PCBP1 depletion enhances sorafenib sensitivity by repressing the proliferation, migration, and invasion of HCC cells

Considering the negative correlation between PCBP1 expression and sorafenib sensitivity, we hypothesized that PCBP1 downregulation would enhance HCC cells' sensitivity to sorafenib. We first transiently knocked down PCBP1 in sorafenib-sensitive Huh7 cells using siRNA (Supplementary Fig. S1A) and found that transient PCBP1 downregulation markedly promoted sorafenib-induced cell death (Fig. 2A). To distinguish transient, siRNA-imposed adaptations from persistent, cell-endogenous interdependencies, we established stable PCBP1-knockdown Hep3B and Huh7 cells using shRNA (Supplementary Fig. S1B). Both transient and stable PCBP1 knockdown consistently sensitized sorafenib-induced cell death in Hep3B and Huh7 cells,

407 respectively (Fig. 2B; Supplementary Figs. S1C-E). Notably, stable PCBP1 knockdown
408 significantly reduced the sorafenib IC_{50} in Hep3B and Huh7 cells (Fig. 2C).
409 Since drug resistance is often correlated with tumor progression, we assessed the effect
410 of PCBP1 knockdown on HCC cell proliferation, migration, and invasion. Colony
411 formation assays showed that PCBP1 knockdown reduced the number of colonies in
412 Hep3B and Huh7 cells, respectively (Fig. 2D; Supplementary Fig. S1F). Wound healing
413 assays revealed that PCBP1 knockdown slowed wound closure (Fig. 2E;
414 Supplementary Fig. S1G). Transwell assays further demonstrated that PCBP1
415 knockdown likely inhibited migration and invasion (Figs. 2F, G). As Hep3B cells have
416 a large size and low intrinsic invasiveness(Liu et al. 2022), we examined the
417 invasiveness using a cell migration assay in zebrafish. Hep3B cells with PCBP1
418 knockdown showed an evident reduction in migration distance and migrated cell
419 number from the yolk sac (Fig. 2H). To explore the mechanism underlying reduced
420 events, we analyzed EMT-related proteins and observed that PCBP1 depletion
421 upregulated the epithelial marker E-Cadherin and downregulated the mesenchymal
422 markers Snail and Vimentin (Fig. 2I), indicating that PCBP1 suppression inhibits EMT.
423 Together, our results showed that PCBP1 downregulation can impede the proliferative,
424 migratory, and invasive capabilities of HCC cells, suggesting a tumor-promoting and
425 drug resistance feature of PCBP1 in HCC.

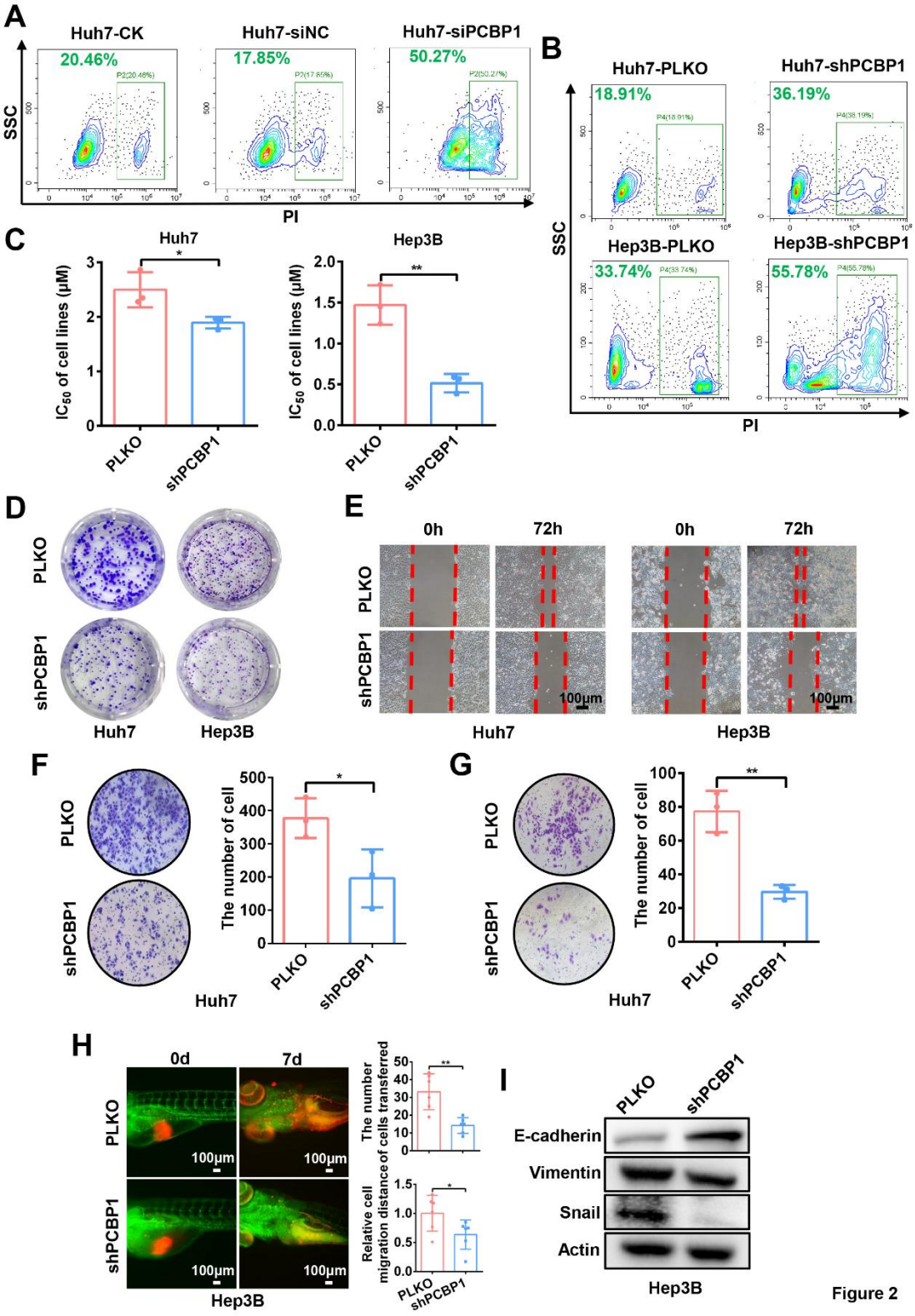


Figure 2

Figure. 2 PCBP1 depletion enhances sorafenib sensitivity via inhibiting the proliferation, migration, and invasion of HCC cells.

(A) Cell death rates of three groups of Huh7 cells after sorafenib treatment (10 μM, 36

h) were detected by flow cytometry. **(B)** Cell death rates of Huh7 (10 μM, 36 h) and Hep3B (10 μM, 48 h) cells after sorafenib treatment were measured by flow cytometry. **(C)** IC_{50} values of sorafenib treatment of Huh7 and Hep3B cells before and after stable PCBP1 knockdown (n = 3). **(D)** Analysis of colony formation ability of HCC cells before and after PCBP1 downregulation. **(E)** Wound-healing assay of HCC cells before and after PCBP1 downregulation. **(F, G)** Analysis and quantification (n = 3) of migration (F) and invasion (G) abilities of Huh7 cells before and after PCBP1 downregulation by transwell migration and invasion assays. The number of seeded cells was 5×10^4 per well, with migration time 24 h and invasion time 48 h. **(H)** In vivo analysis of migration ability of Hep3B cells before and after PCBP1 downregulation using a zebrafish model; the number and distance of cells migrating out of the yolk sac were quantified (n = 6). **(I)** Expression of EMT-related proteins in Hep3B cells before and after PCBP1 downregulation were detected by western blot. $*P < 0.05$, $**P < 0.01$.

PCBP1 downregulation renders sorafenib sensitivity via apoptosis rather than ferroptosis

Given that sorafenib exerts its cytotoxic effect through multiple mechanisms, including apoptotic, autophagic, and ferroptosis, we sought to clarify which cell death type occurs in PCBP1-mediated sorafenib sensitization. Liperfluo staining showed that sorafenib treatment induced lipid peroxidation, a hallmark of ferroptosis, exhibiting a fluorescence shift in both HCC cells (Fig. 3A), which is consistent with previous reports(Li et al. 2023). PCBP1 knockdown slightly increased intracellular Fe^{2+} levels

(Fig. 3B), but had no effect on the expression of ferritin heavy chain (FTH1), a key regulator of iron homeostasis (Fig. 3C). MDA levels—another marker of lipid peroxidation, were no unchanged between PCBP1-knockdown and parental cells upon sorafenib treatment (Fig. 3D). Moreover, we treated cells with the ferroptosis inducer RSL3 and inhibitor Fer-1 and observed that RSL3 induced a distinct ferroptotic morphology from that in sorafenib-induced cell death, and PCBP1 knockdown did not alter RSL3 sensitivity either (Figs. 3E, F). Additionally, Fer-1 failed to reverse the enhanced sorafenib sensitivity in PCBP1-knockdown cells (Supplementary Figs. S2A, B), excluding ferroptosis as the main cell death manner by sorafenib.

We next assessed whether autophagy or apoptosis is involved in this sorafenib-induced cell death. PCBP1 knockdown did not change the expression of LC3B-I/II, a marker of autophagosome formation and P62, a marker of autophagic flux (Fig. 3G), ruling out the autophagic cell death. In contrast, immunoblots manifested the increases of cleaved Caspase-3, cleaved PARP and p-H2AX, markers of apoptosis (Figs. 3G, H). Cytometry analysis similarly exhibited an evidently enhanced sorafenib-induced apoptosis in PCBP1 knockdown cells, in comparison with the parental ones (Fig. 3I). Treatment with the pan-caspase inhibitor Z-VAD-FMK blocked this cell death (Supplementary Figs. S2C, D). Collectively, these data demonstrate that PCBP1-mediated sorafenib sensitization is mainly through apoptosis, rather than ferroptosis or autophagy.

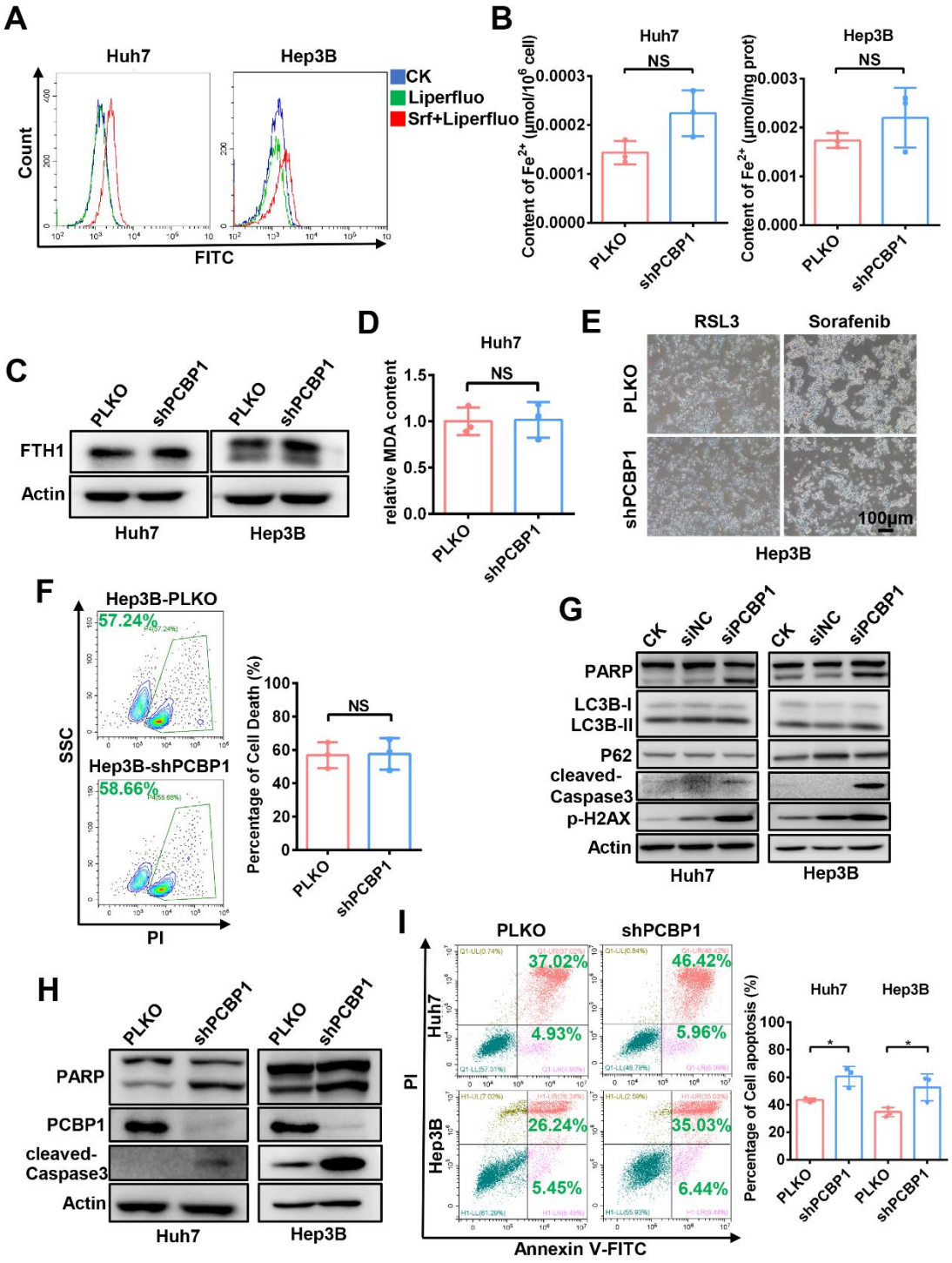


Figure 3

Figure. 3 PCBP1 downregulation enhances sorafenib-induced apoptosis of HCC cells.

(A) Flow cytometric analysis of intracellular lipid peroxidation in HCC cells before and after sorafenib treatment using Liperfluo (1 μM) staining. **(B)** Detection and quantification (n = 3) of intracellular Fe^{2+} concentration in HCC cells before and after stable PCBP1 downregulation. **(C)** Protein expression levels of FTH1 in HCC cells before and after stable PCBP1 downregulation. **(D)** Measurement of MDA content (n = 3) in Huh7 cells after sorafenib treatment (10 μM, 36 h). **(E)** Bright-field morphology of Hep3B cells after treatment with RSL3 (500 nM, 48 h) or sorafenib (10 μM, 48 h). **(F)** Flow cytometric analysis of cell death rate (n = 3) of Hep3B cells after RSL3 (500 nM, 48 h) treatment. **(G)** Expression levels of apoptosis- and autophagy-related proteins in cells before and after transient PCBP1 knockdown following sorafenib treatment (10 μM; 36 h for Huh7 and 48 h for Hep3B). **(H)** Expression levels of apoptosis-related proteins of Huh7 and Hep3B cells before and after stable PCBP1 downregulation following sorafenib treatment (10 μM; 36 h for Huh7 and 48 h for Hep3B). **(I)** Flow cytometric analysis of apoptosis rate (n = 3) of Huh7 and Hep3B cells after sorafenib treatment (10 μM; 48 h). Srf represents sorafenib. *$P < 0.05$.

Transient PCBP1 downregulation enhances immediate sorafenib sensitivity via repressing BAG1-p36 translation

To dissect the molecular mechanism of PCBP1 depletion-induced apoptosis, we first checked and confirmed that PCBP1 knockdown alone did not affect either autophagy or apoptosis (Supplementary Fig. S3A) and that sorafenib treatment in turn did not alter PCBP1 expression (Supplementary Fig. S3B), indicating that PCBP1 depletion acts

upstream of sorafenib-induced apoptosis. Given the binding of PCBP1 to the IRES of *BAG1* mRNA in enhancing its translation activity in CAMA-1 and HeLa cells(Pickering et al. 2003), and the coexistence of low PCBP1 and high BAG1 in some tumors(Fan et al. 2021, Zheng et al. 2022), we thus explored whether PCBP1 modulates BAG1 in HCC. Analysis of The Human Protein Atlas (HPA) showed that BAG1 is upregulated in HCC tissues, potentially related to elevated PCBP1 expression (Supplementary Fig. S3C). Meanwhile, *BAG1*-high patients exhibited poorer survival, although without statistical significance (Supplementary Fig. S3D), suggestive of a correlation between PCBP1 and BAG1 in HCC.

BAG1 is composed of four isoforms translated from a single mRNA, among which the initiation codon AUG for BAG1-p36, along with an extra IRES, heavily suppresses the following BAG1-p29 translation (Fig. 4A)(Hou et al. 2024). Our results verified that BAG1-p36 is the predominant isoform in four HCC cell lines (Supplementary Fig. S3E). Transient PCBP1 knockdown reduced BAG1-p36 protein level, but did not affect BAG1-p50 or BAG1-p46 (Fig. 4B), indicating the pivotal role of BAG1-p36 in PCBP1 depletion-induced cell death upon sorafenib treatment. We thus knock down BAG1 alone and noted the increase in the cleavage of Caspase-3 and PARP and cell death by sorafenib treatment, without a change in autophagy markers (Fig. 4C; Supplementary Fig. S3F).

To confirm that BAG1-p36 mediates PCBP1-dependent sorafenib sensitivity, we forced expression of BAG1-p36 in PCBP1-depleted cells and observed the decrease in the cleavages of Caspase-3 and PARP (Fig. 4D; Supplementary Fig. S3G) and cell death

518 (Fig. 4E; Supplementary Fig. S3H). Notably, *BAG1* mRNA level exhibited no change,
519 with PCBP1 expression alteration (Fig. 4F). TCGA data analysis also revealed no
520 correlation between *PCBP1* and *BAG1* mRNA (Fig. 4G), indicating the post-
521 transcriptional regulation of BAG1 by PCBP1.
522 To determine the effect of PCBP1 in BAG1-p36 translation or degradation, we treated
523 cells with a proteasome inhibitor, MG132, or a translation inhibitor, CHX, after
524 siPCBP1 treatment (36 h for Huh7; Supplementary Figs. S3I-J). MG132 treatment
525 induced reduced BAG1-p36 accumulation in PCBP1 knockdown cells, compared with
526 the parental cells at each indicated time point (Fig. 4H). In contrast, CHX treatment
527 exerted no influence on the BAG1-p36 degradation rate (Fig. 4I), ruling out effects of
528 PCBP1 depletion on protein stability. As PCBP1 can bind the *BAG1* mRNA IRES, we
529 performed a RIP assay in Huh7 cells and confirmed the binding of *BAG1* mRNA with
530 PCBP1 (Fig. 4J). Collectively, these results demonstrate that transient PCBP1
531 downregulation enhances sorafenib-induced apoptosis by impeding BAG1-p36
532 translation efficiency.

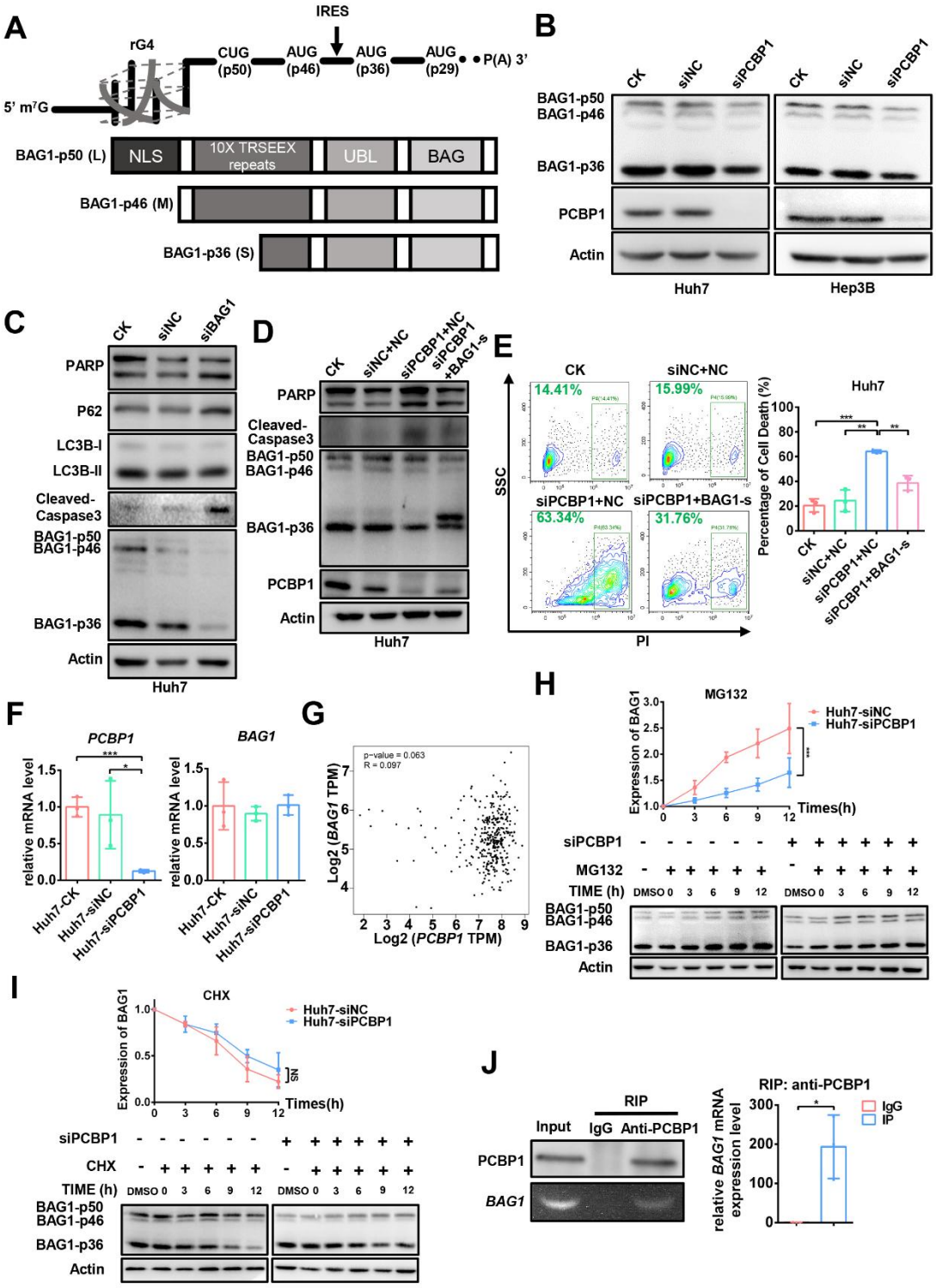


Figure 4

Figure. 4 Transient PCBP1 silence represses the translation of BAG1-p36 and enhances sorafenib sensitivity of HCC cells.

(A) Schematic representation of structures of *BAG1* mRNA and its protein isoforms.

(B) Expression levels of BAG1 protein in Huh7 cells before and after transient PCBP1 knockdown showing reduced BAG1-p36 expression. **(C)** Expression levels of apoptosis- and autophagy-related proteins in Huh7 cells before and after transient BAG1 knockdown (50 nM siRNA) treated with sorafenib (10 μM, 36 h). **(D)** Changes of apoptosis-related proteins in Huh7 cells after transient PCBP1 knockdown and BAG1-p36 restoration following sorafenib treatment (10 μM, 36 h). **(E)** Flow cytometric analysis of cell death rate (n = 3) of Huh7 cells after transient PCBP1 knockdown and BAG1-p36 restoration under sorafenib treatment (10 μM, 36 h). **(F)** Expression levels of *BAG1* mRNA (n = 3) in Huh7 cells before and after transient PCBP1 knockdown. **(G)** Correlation analysis of *PCBP1* mRNA and *BAG1* mRNA expression in HCC tissues based on TCGA database. **(H)** Accumulation levels of BAG1-p36 protein (n = 3) in Huh7 cells before and after transient PCBP1 knockdown following MG132 (10 μM) treatment were detected by western blot. **(I)** Degradation levels of BAG1-p36 protein (n = 3) in Huh7 cells before and after transient PCBP1 knockdown following cycloheximide (CHX, 50 μg/ml) treatment were detected by western blot. **(J)** Verification of the binding of PCBP1 with *BAG1* mRNA (n = 3) in Huh7 cells by RNA immunoprecipitation (RIP) assay. $*P < 0.05$, $**P < 0.01$, $***P < 0.001$.

Adaptive recovery of decreased BAG1-p36 expression is mediated by compensatory PTBP1 upregulation upon long-term PCBP1 depletion

With the stable PCBP1 knockdown by PCBP1-specific shRNA over time, the reduced

559 BAG1-p36 protein level unexpectedly recovered (Fig. 5A), in comparison with the
560 transient PCBP1 with the same shRNA (Fig. 5B), indicating adaptive upregulation of
561 BAG1-p36 in PCBP1-depleted cells. Likewise, cells with the stable PCBP1-
562 knockdown became less sensitive to sorafenib than with the transient PCBP1
563 knockdown (Fig. 5C), and a second BAG1 knockdown could increase sorafenib
564 sensitivity in those long stable PCBP1-knockdown cells again (Fig. 5D; Supplementary
565 Fig. S4A), suggesting that long-term PCBP1 knockdown-mediated sorafenib
566 sensitivity is independent of the immediate BAG1 downregulation.
567 Given that compensatory feedback exists among disparate genes and protein
568 products(Ma et al. 2019), we hypothesized compensatory upregulation of other RNA-
569 binding proteins counteracts PCBP1 functional loss after sustained knockdown. PTBP1
570 also binds to the IRES region of BAG1 mRNA. We thus detected and found the
571 markedly increased PTBP1protein level upon stable PCBP1 knockdown (Fig. 5E). To
572 verify the regulation of BAG1-p36 expression by PTBP1, we performed the forced
573 PTBP1 expression change and showed that PTBP1 knockdown reduced BAG1-p36
574 expression (Fig. 5F), while PTBP1 overexpression elevated BAG1-p36 levels (Fig. 5G).
575 We further examined the relevance of PTBP1 expression and sorafenib sensitivity.
576 Results showed that PTBP1 knockdown rendered HCC cells more sensitive to sorafenib
577 and increased apoptosis-related protein levels in HCC cells. In contrast, PTBP1
578 overexpression attenuated cell sensitivity to sorafenib with the decreased levels of
579 apoptosis-related proteins (Figs. 5H-J), which mimicked the function of PCBP1.
580 To uncover the mechanism underlying the upregulation and function of PTBP1, we

581 determined *PTBP1* mRNA expression and observed a significant increase in Hep3B
582 cells (Fig. 5K). Furthermore, Huh7 cells with PTBP1 knockdown were treated with
583 MG132. The results showed that PTBP1 knockdown markedly reduced BAG1-p36
584 translation without obvious time-dependent accumulation, consistent with PCBP1
585 function (Fig. 5L). Altogether, PTBP1 compensates for the loss of PCBP1 function and
586 modulates BAG1-p36 expression as well as sorafenib sensitivity in HCC cells.

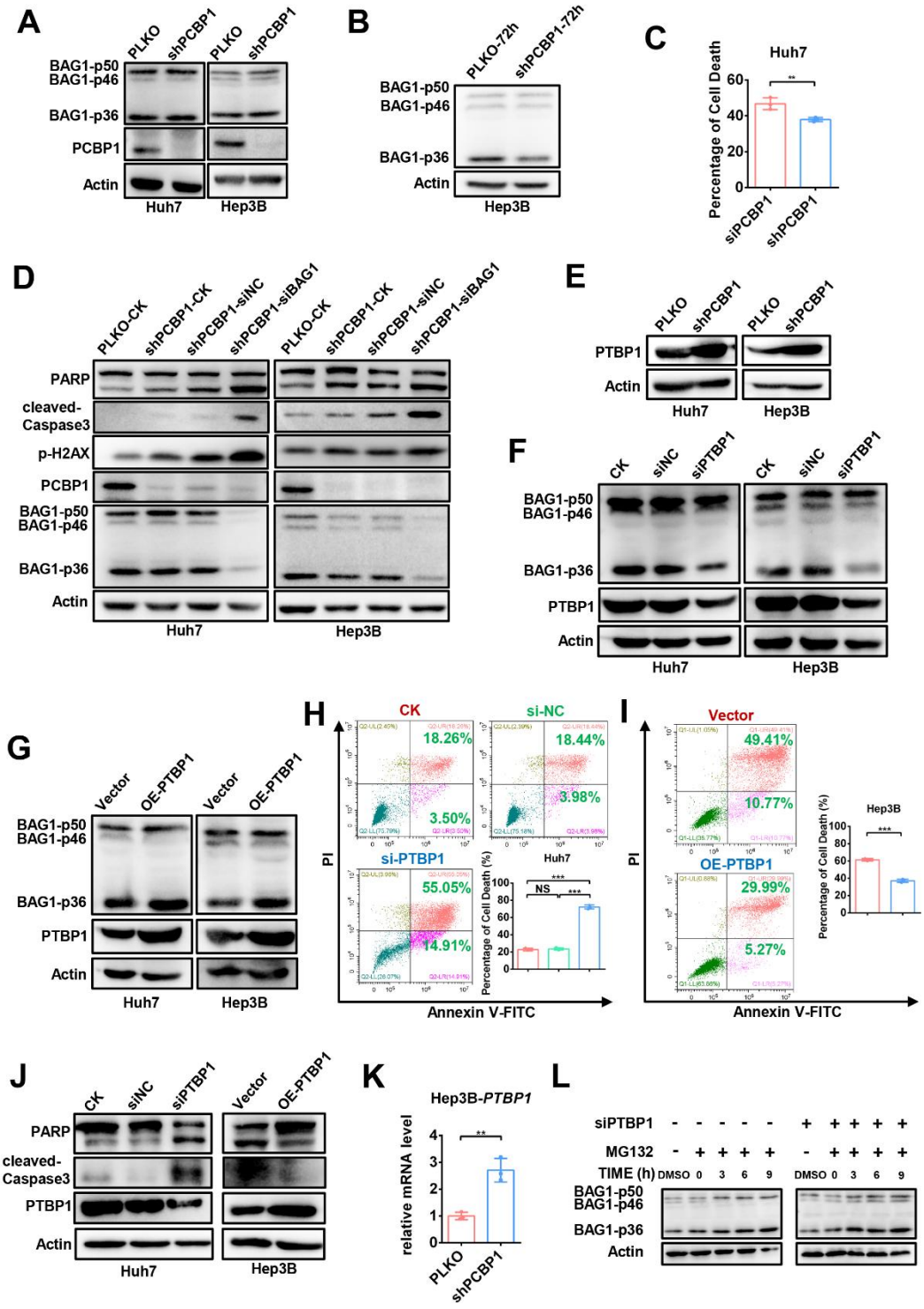


Figure 5

Figure. 5 PTBP1 drives adaptive recovery of BAG1-p36 in long-term PCBP1 knockdown cells.

(A) Protein expression levels of BAG1 in HCC cells before and after stable PCBP1

591 downregulation. **(B)** Protein expression levels of BAG1 in Hep3B cells 72 h after
592 transfection with the PLKO-shPCBP1 plasmid. **(C)** Analysis of cell death rates of HCC
593 cells after transient and stable downregulation of PCBP1 with sorafenib treatment (n=
594 3). **(D)** Expression levels of apoptosis-related proteins in Huh7 (10 μM, 36 h) and
595 Hep3B (10 μM, 48 h) cells after sorafenib treatment with stable PCBP1 knockdown,
596 before and after an additional transient BAG1 knockdown. **(E)** Protein expression
597 levels of PTBP1 in HCC cells before and after stable PCBP1 downregulation. **(F-G)**
598 Protein expression levels of BAG1 before and after transient PTBP1 knockdown (50
599 nM siRNA) or PTBP1 overexpression. **(H-I)** Flow cytometric analysis of apoptosis rate
600 (n = 3) of Huh7 and Hep3B cells before and after PTBP1 downregulation or
601 overexpression following sorafenib treatment (10 μM; 36 h for Huh7 and 48 h for
602 Hep3B). **(J)** Expression levels of apoptosis-related proteins of Huh7 and Hep3B cells
603 before and after PTBP1 downregulation or overexpression following sorafenib
604 treatment (10 μM; 36 h for Huh7 and 48 h for Hep3B). **(K)** Expression levels of *PTBP1*
605 mRNA (n = 3) in Hep3B cells before and after stable PCBP1 downregulation. **(L)**
606 Accumulation levels of BAG1-p36 protein in Huh7 cells before and after transient
607 PTBP1 knockdown following MG132 (10 μM) treatment were detected by western blot.
608 $^{**}P < 0.01$, $^{***}P < 0.001$.
609
610 **Long-term PCBP1 depletion enhances sorafenib sensitivity via decreasing the**
611 ***SOX2* mRNA stability and translation**
612 To identify the potent downstream targets for sorafenib sensitivity upon long-term

PCBP1 knockdown, we performed RNA-seq in the long-term PCBP1 knockdown and control Hep3B cells, and identified downregulation of AFP, VIM, and other oncogenes, accompanied by enriched genes in TGFβ, PI3K/Akt, and Wnt/β-catenin pathways (Fig. 6A; Supplementary Figs. S4B-D). Protein-protein interaction (PPI) network analysis identified SOX2, a key transcription factor for stemness maintenance, as a core node (Fig. 6B; Supplementary Fig. S4E). Consistently, both transient and stable PCBP1 knockdown decreased SOX2 expression in Hep3B and LM3 cells, which was restored by PCBP1 re-expression (Figs. 6C, D; Supplementary Fig. S5A), indicating that PCBP1 regulates SOX2 regardless of knockdown time duration.

PCBP1 depletion has been shown to enhance cancer cell stemness by modulating CD44 splicing, and activation of the TGFβ pathway also promotes stemness by suppressing PCBP1-dependent CD44 splicing(Tripathi et al. 2016). We thus checked them and found that PCBP1 knockdown did not alter TGFβ signaling or CD44 splicing in HCC cells (Supplementary Figs. S5B, C). In contrast, SOX2 knockdown increased sorafenib sensitivity (Figs. 6E, F; Supplementary Fig. S5D), whereas either transient or stable SOX2 re-expression could rescue the PCBP1 knockdown-induced cell death (Figs. 5G, H; Supplementary Figs. S5E, F), confirming that PCBP1/SOX2 axis downregulation mediates drug response.

Reciprocal regulation between SOX2 and PI3K/Akt pathway is observed in different tumors(Guo et al. 2025, Yang et al. 2025), which was consistent with our KEGG analysis. We examined whether the PI3K/Akt pathway is involved in SOX2 regulation. Akt inhibitor MK-2206 reduced SOX2 levels and enhanced sorafenib sensitivity

(Supplementary Figs. S5G, H), confirming PI3K/Akt as an upstream regulator of SOX2. However, PCBP1 knockdown did not affect Akt or mTOR phosphorylation (Supplementary Fig. S5I), indicating that PCBP1 regulates SOX2 independently of PI3K/Akt. We then assessed transcriptional and post-transcriptional regulation and noted that *SOX2* mRNA levels were reduced in Hep3B, but unchanged in LM3 cells (Fig. 6I). Blockade of new RNA synthesis with Actinomycin D (ACTD) treatment revealed that PCBP1 knockdown shortened *SOX2* mRNA half-life in Hep3B (Fig. 6J), indicating reduced mRNA stability. In LM3 cells, PCBP1 knockdown reduced both SOX2 translation and degradation upon MG132 and CHX treatments (Fig. 6K), indicating cell context-specific post-transcriptional regulation. As PCBP1 is an RNA-binding protein, we verified the interaction between PCBP1 and *SOX2* mRNA. RIP assays confirmed such binding in both cell lines (Fig. 6L), and RBPmap analysis predicted multiple potential PCBP1-binding sites in the *SOX2* mRNA 5'-UTR or 3'-UTR (Supplementary Table S4)(Paz et al. 2022). These data demonstrate that PCBP1 regulates SOX2 via cell type-specific post-transcriptional mechanisms (mRNA stability or translation), depending on the cellular context.

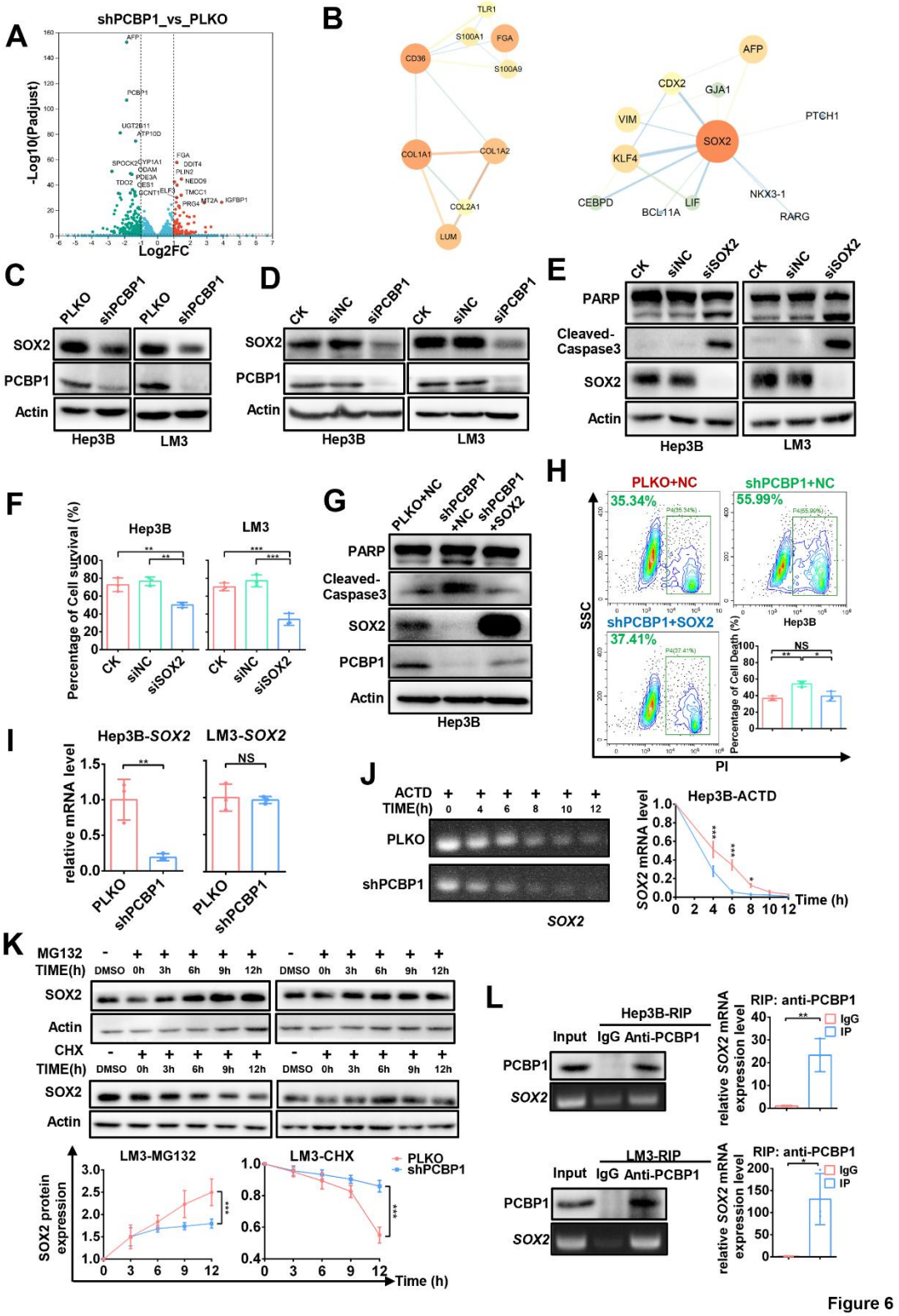


Figure 6

Figure. 6 Stable PCBP1 downregulation enhances sorafenib sensitivity of HCC cells by suppressing SOX2 expression.

(A) Volcano plot of genes regulated by stable PCBP1 downregulation. Red indicates

upregulated genes, green indicates downregulated genes, and blue indicates genes without significant change. **(B)** Core protein–protein interaction network of differentially expressed genes regulated by stable PCBP1 downregulation compared with the control group. **(C-D)** Protein expression levels of SOX2 in HCC cells before and after both stable and transient PCBP1 knockdown. **(E)** Expression levels of apoptosis-related proteins in Hep3B (10 μM, 48 h) and LM3 (10 μM, 36 h) cells before and after transient SOX2 knockdown (50 nM siRNA) following sorafenib treatment. **(F)** Quantification of cell adhesion (n = 3) of Hep3B and LM3 cells before and after transient SOX2 knockdown under sorafenib treatment (10 μM; 48 h for Hep3B and 36 h for LM3). **(G, H)** Changes of apoptosis-related proteins (G) and quantification of cell death rates (H, n = 3) of Hep3B cells after stable PCBP1 downregulation and SOX2 restoration following sorafenib treatment (10 μM, 48 h). **(I)** Expression levels of *SOX2* mRNA (n = 3) in HCC cells before and after stable PCBP1 downregulation. **(J)** Degradation rates of *SOX2* mRNA (n = 3) in Hep3B cells treated with actinomycin D (ACTD, 5 μg/mL) before and after stable PCBP1 downregulation. **(K)** Analysis of SOX2 protein accumulation and degradation (n = 3) in LM3 cells treated with MG132 (15 μM) and cycloheximide (CHX, 50 μg/mL) before and after stable PCBP1 downregulation. **(L)** RIP assay verifying the binding of PCBP1 with *SOX2* mRNA (n = 3) in Hep3B and LM3 cells. *$P < 0.05$, **$P < 0.01$, ***$P < 0.001$.

SOX2 mediates PCBP1's role in sorafenib resistance through β-catenin pathway

As our KEGG analysis of RNA-seq in PCBP1 knockdown cells also highlighted the

enrichment of genes in the Wnt/β-catenin pathway, and SOX2 activates the Wnt/β-catenin pathway in colorectal cancer(Zhu et al. 2021), we sought to know whether SOX2 mediates PCBP1's role through this signalling in HCC. Our experiment results revealed that either PCBP1 or SOX2 knockdown reduced β-catenin protein (Figs. 7A, B), and such reduction could be reversed by forced SOX2 expression (Fig. 7C; Supplementary Fig. S6A). Immunofluorescence further confirmed that PCBP1 knockdown reduced SOX2 and β-catenin levels (Fig. 7D). TCGA data analysis showed a positive correlation between *PCBP1* and *β-catenin* mRNA (Fig. 7E), and RT-qPCR revealed that the β-catenin inhibitor, *DKK1*, was upregulated in PCBP1-knockdown cells (Supplementary Fig. S6B), suggesting that PCBP1/SOX2 may regulate β-catenin via DKK1. To confirm that β-catenin mediates sorafenib sensitivity, we treated cells with the β-catenin inhibitor XAV-939. XAV-939 enhanced sorafenib sensitivity (Fig. 7F), mimicking the effect of PCBP1 or SOX2 knockdown.

SOX2 re-expression restored the reduced colony-forming ability of Hep3B cells from PCBP1 knockdown (Supplementary Fig. S6C). To verify these in vivo, we established a subcutaneous xenograft model using Hep3B cells (Fig. 7G). PCBP1 knockdown slowed tumor growth (Fig. 7H). Sorafenib treatment further inhibited tumor growth in PCBP1-knockdown cells (Figs. 7I-K), confirming the enhanced efficacy of sorafenib. Notably, SOX2 re-expression reversed the tumor-suppressive effect and drug sensitivity from PCBP1 knockdown (Figs. 7H-K), validating the PCBP1/SOX2/β-catenin axis in vivo.

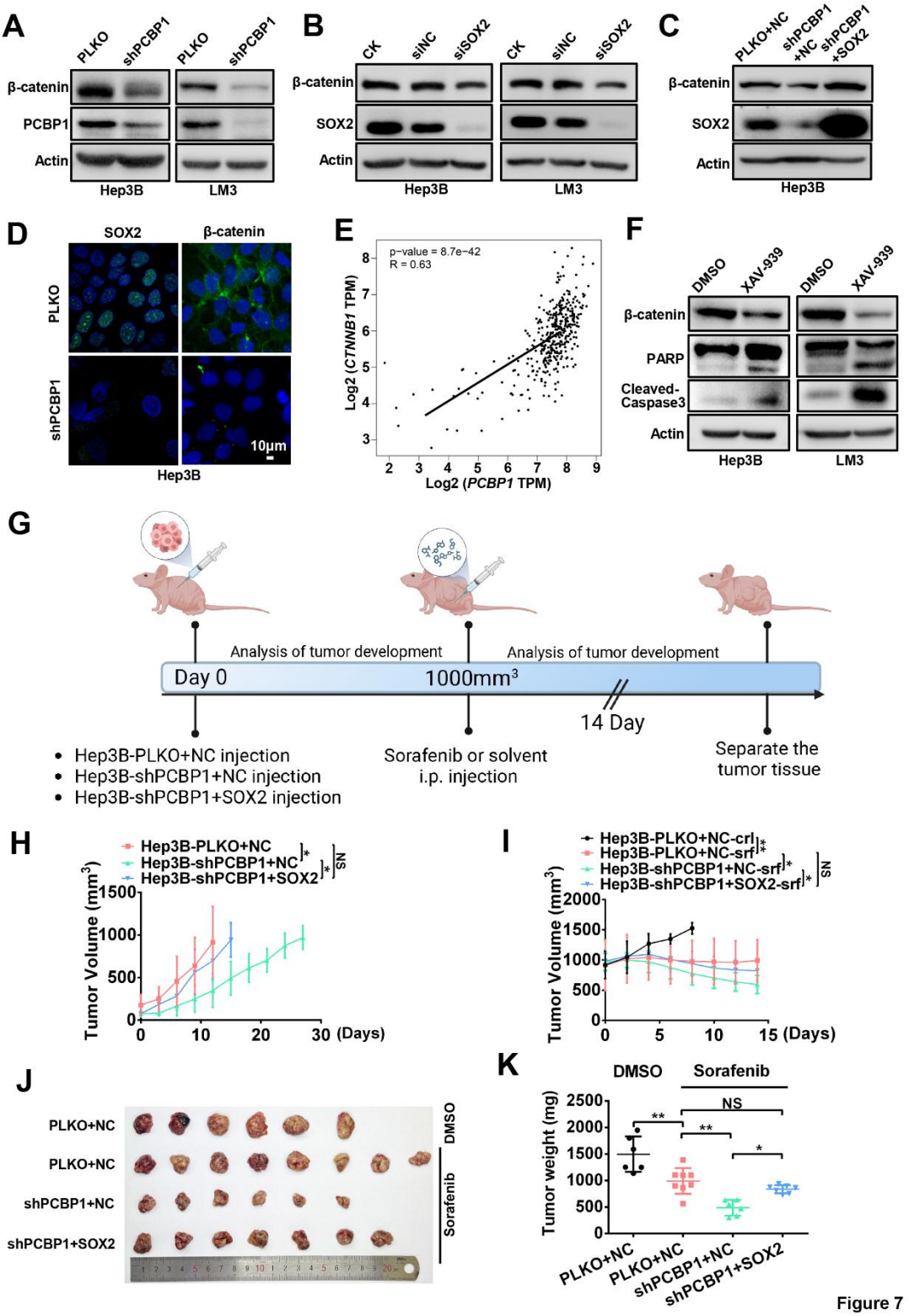


Figure 7

Figure. 7 Inhibition of the PCBP1/SOX2/β-catenin axis enhances sorafenib sensitivity of HCC cells.

(A) Protein expression levels of β-catenin in HCC cells before and after stable PCBP1

knockdown. **(B)** Protein expression levels of β-catenin in HCC cells before and after transient SOX2 knockdown. **(C)** Protein expression levels of β-catenin in HCC cells after stable PCBP1 knockdown and SOX2 restoration. **(D)** Immunofluorescence analysis of the expression of SOX2 and β-catenin in HCC cells before and after stable PCBP1 knockdown. **(E)** Correlation analysis of mRNA expression of *PCBP1* and *CTNNB1* in HCC tissues based on TCGA database. **(F)** Expression levels of apoptosis-related proteins in Hep3B and LM3 cells treated with sorafenib alone (10 μM) or in combination with the β-catenin inhibitor XAV-939 (20 μM). **(G)** Schematic diagram of subcutaneous xenograft formation and drug administration in nude mice. **(H)** Tumor growth curves ($n \geq 6$) of subcutaneous xenograft models of nude mice. **(I)** Tumor regression curves ($n \geq 6$) of xenograft models after sorafenib treatment. **(J)** Photographs of excised tumors ($n \geq 6$). **(K)** Statistical analysis of tumor weights ($n \geq 6$) after harvesting at the end of the experiment. $^{*}P < 0.05$, $^{**}P < 0.01$.

Dual targeting of BAG1 and SOX2 enhances and prolongs the cytotoxic effect of sorafenib

Given that the stable PCBP1 knockdown triggers BAG1-p36 adaptive recovery, we hypothesized that simultaneous targeting of BAG1 and SOX2 would sustain sorafenib sensitivity. We established BAG1/SOX2 double-knockdown Hep3B cells (Fig. 8A). In comparison, single PCBP1 knockdown resulted in BAG1-p36 recovery after 4 weeks, with sorafenib sensitivity decrease, while dual BAG1/SOX2 knockdown maintained BAG1-p36 at low levels and sustained sorafenib-induced cell death (Figs. 8B, C). To

validate the association between gene expression and drug sensitivity in clinical specimens, we collected HCC tumor tissues from six postoperative patients treated with lenvatinib, a first-line targeted agent with targets overlapping those of sorafenib(Llovet et al. 2021). Three patients developed recurrence after a period of treatment, whereas the remaining three have not recurred to date. PCBP1, BAG1, and SOX2 were expressed at higher levels in tumors from the recurrent group (Fig. 8D). These data indicated that dual targeting of BAG1 and SOX2 would be efficient to sustain the efficacy of sorafenib therapy in PCBP1-overexpressing HCC (Fig. 8E).

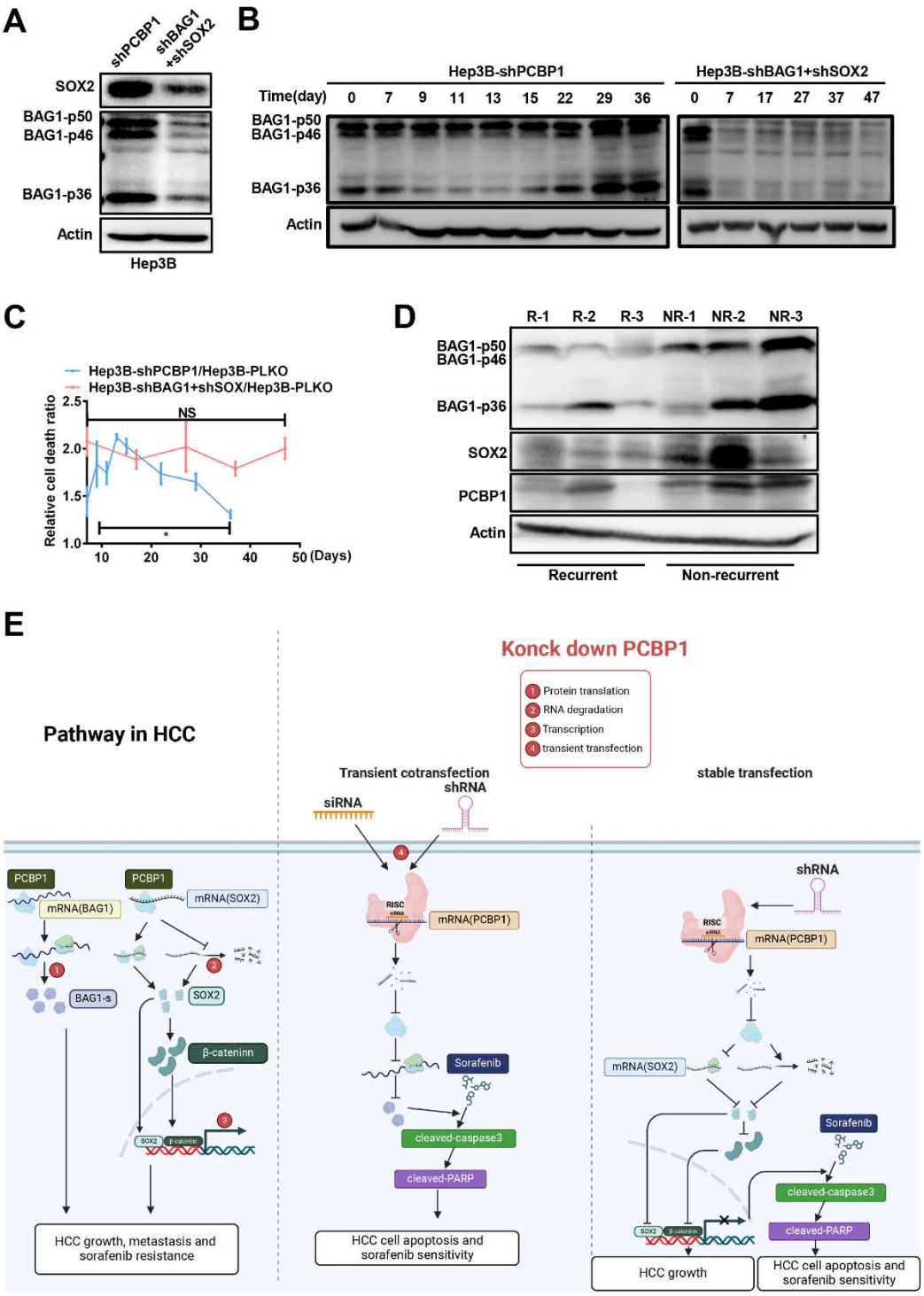


Figure 8

Figure. 8 Double knockdown of BAG1 and SOX2 effectively prolongs the cytotoxic effect of sorafenib on HCC cells.

(A) Western blot validation of BAG1 and SOX2 double-knockdown Hep3B cells. **(B)**

Verification of BAG1 restoration of HCC cells after single PCBP1 knockdown and double BAG1/SOX2 knockdown. **(C)** Flow cytometric analysis of changes of cell death rates (n =3) of HCC cells after single PCBP1 knockdown and double BAG1/SOX2 knockdown following sorafenib (10 μM, 48 h) treatment. **(D)** Protein expression levels of PCBP1, BAG1, and SOX2 in the recurrent and non-recurrent HCC groups after lenvatinib treatment. **(E)** Schematic illustration of the mechanism by which downregulation of PCBP1 enhances sorafenib sensitivity of HCC cells through dual inhibition of the BAG1 and SOX2/β-catenin axes.

Discussion

Clinically, only about 30% of HCC patients respond to sorafenib, and even responsive patients often develop acquired resistance within 6 months(Tang et al. 2020). Thus, dissecting the underlying intrinsic and acquired resistance-related genes is crucial for sorafenib efficacy and prolonged clinical utilization. Here, we identify that PCBP1 functions as a key culprit of tumor development and intrinsic sorafenib resistance in HCC in a context-dependent manner, unlike its tumor suppressor function in prostate and colorectal cancers by repressing autophagy to induce apoptosis(Zhang et al. 2016, Zhang et al. 2018). Our results demonstrate that PCBP1 downregulation exerts straightforward pro-apoptosis rather than pro-ferroptosis by reducing BAG-p36 and SOX2 expression upon sorafenib treatment. Meanwhile, bioinformatics analysis show that PCBP1 is upregulated in sorafenib-insensitive HCC tissues and correlates with poor prognosis, rendering it a potential prognostic marker for proper drug usage and a

possible therapeutic target.

Unexpectedly, PCBP1 depletion shows a time-dependent dual regulatory role in sorafenib sensitization in HCC by transiently inhibiting BAG1-p36 translation to promote apoptosis, while continuously suppressing the SOX2/β-catenin axis to attenuate CSC properties. This time-dependent mechanism reflects the adaptive response in tumor cells to long-term drug usage or oncogene targeting, as in prolonged PCBP1 knockdown cells, BAG1-p36 could be adaptively recovered, a phenomenon initiated by the upregulation of another RNA-binding protein PTBP1. As the adaptive resistance is common for long-term drug application, our results thus indicate that the recovery of BAG1-p36 would be an important player to orchestrate the acquired drug resistance of sorafenib in HCC, even in other types of tumors(Zhang et al. 2016, Townsend et al. 2003). Therefore, drugs that maintain BAG1 suppression may sustain sorafenib sensitivity. Importantly, PCBP1 reduction not only transiently decreased BAG1-p36 but also downregulated SOX2, preserving sorafenib sensitivity even after BAG1 recovery. Thus, the simultaneous inhibition of BAG1 with SOX2 could maintain BAG1 suppression and sustain sorafenib sensitivity in PCBP1 highly expressing HCC. Finally, using clinical HCC specimens, we validated the association of PCBP1, BAG1, and SOX2 expression with tumor drug resistance, consistent with our cell-based findings. Although the samples were obtained from patients treated with lenvatinib, its therapeutic targets overlap with those of sorafenib(Llovet et al. 2021), supporting the relevance of these results.

PCBP1 enhances *BAG1* IRES activity in certain tumors(Pickering et al. 2003), but no

specific BAG1 isoform is well characterized for anti-apoptosis or drug resistance in HCC. Here, we disclose that PCBP1, as an upstream regulator, specifically maintain the BAG1-p36 isoform in HCC to clarify the intrinsic sorafenib resistance by BAG1 overexpression(Ni et al. 2013). Furthermore, we disclosed the mechanism underlying the BAG1-p36 expression recovery over long-term PCBP1 depletion and revealed the compensatory upregulation of another RNA-binding protein, PTBP1, for PCBP1 loss. Thus, dual targeting of PCBP1 and PTBP1 may be an effective strategy to overcome sorafenib resistance and sustain therapeutic efficacy. Moreover, PCBP1 downregulation and sorafenib have both been shown to induce ferroptosis in colorectal cancer and head and neck cancer(Lee et al. 2022, Yu et al. 2025), but our results here rule out the ferroptosis occurrence in PCBP1-depletion-initiated sorafenib sensitization. This discrepancy may be due to cell type differences, as HCC cells may rely more on apoptosis than ferroptosis for sorafenib-induced cell death.

Although SOX2/β-catenin activation is documented to induce chemoresistance in colorectal cancer(Tang et al. 2018), we further unveil PCBP1 as an upstream master of SOX2 in HCC via cell line-specific post-transcriptional mechanisms on either mRNA stability or translation efficiency, highlighting the importance of cellular context in RNA-binding protein function and tumor cell heterogeneity(Zhang et al. 2020).

Conclusions

In summary, our study demonstrates that PCBP1 is a key regulator of tumor progression and intrinsic sorafenib resistance by upregulation of BAG1-p36 and activation of the

SOX2/β-catenin pathway to maintain CSC properties in HCC. BAG1-p36 would be a master gene for the acquired drug resistance, especially for sorafenib-like drugs. PCBP1 and PTBP1 would be a prognostic marker and therapeutic target for proper drug utilization, and doubly targeting BAG1 and SOX2 would be an impressive strategy to overcome adaptive and intrinsic sorafenib resistance in PCBP1 highly expressing HCC.

List of abbreviations

ACTD: Actinomycin D

ATCC: American Type Culture Collection

BAG1: Bcl-2–associated athanogene-1

BSA: Bovine serum albumin

CCK-8: Cell Counting Kit-8

CPTAC: Clinical Proteomic Tumor Analysis Consortium

CSC: Cancer stem cell

CHX: Cycloheximide

cDNA: complementary DNA

DEGs: Differentially expressed genes

DMEM: Dulbecco's Modified Eagle Medium

ECL: Enhanced chemiluminescence

EMT: Epithelial-mesenchymal transition

FC: Fold change

FDR: False discovery rate

Fer-1: Ferrostatin-1

FBS: Fetal bovine serum

FTH1: Ferritin heavy chain

GEO: Gene Expression Omnibus

GO: Gene Ontology

HCC: Hepatocellular carcinoma

HPA: The Human Protein Atlas

HRP: Horseradish peroxidase

IC_{50}: Half-maximal inhibitory concentration

IACUC: Institutional Animal Care and Use Committee

ICC: Immunocytochemistry

IRES: Internal ribosome entry site

KEGG: Kyoto Encyclopedia of Genes and Genomes

MDA: Malondialdehyde

OS: Overall survival

PBS: Phosphate-buffered saline

PCBP1: Poly(rC)-binding protein 1

PDGFR: Platelet-derived growth factor receptor

PI: Propidium iodide

PPI: Protein-protein interaction

PTBP1: Polypyrimidine tract-binding protein 1

PVDF: Polyvinylidene difluoride

RFS: Recurrence-free survival

RIP: RNA immunoprecipitation

RIN: RNA Integrity Number

RNA-seq: RNA sequencing

RT-qPCR: Real-time quantitative PCR

SDS-PAGE: Sodium dodecyl sulfate-polyacrylamide gel electrophoresis

SD: Standard deviation

shRNA: short hairpin RNA

siRNA: small interfering RNA

SOX2: Sex-determining region Y-box 2

STR: Short tandem repeat

TBST: Tris-buffered saline with Tween-20

TCGA: The Cancer Genome Atlas

VEGFR: Vascular endothelial growth factor receptor

WB: Western blot

References

1. Bray F, Laversanne M, Sung H, Ferlay J, Siegel RL, Soerjomataram I*, et al.* Global cancer statistics 2022: GLOBOCAN estimates of incidence and mortality worldwide for 36 cancers in 185 countries. CA Cancer J Clin. 2024; 74(3): 229-263.

2. Petrick JL, Florio AA, Znaor A, Ruggieri D, Laversanne M, Alvarez CS*, et al.*

International trends in hepatocellular carcinoma incidence, 1978-2012. Int J Cancer. 2020; 147(2): 317-330.

3. Tang W, Chen Z, Zhang W, Cheng Y, Zhang B, Wu F*, et al.* The mechanisms of sorafenib resistance in hepatocellular carcinoma: theoretical basis and therapeutic aspects. Signal Transduct Target Ther. 2020; 5(1): 87.

4. Li Q, Chen K, Zhang T, Jiang D, Chen L, Jiang J*, et al.* Understanding sorafenib-induced ferroptosis and resistance mechanisms: Implications for cancer therapy. Eur J Pharmacol. 2023; 955: 175913.

5. Prieto-Dominguez N, Ordonez R, Fernandez A, Garcia-Palomo A, Muntane J, Gonzalez-Gallego J*, et al.* Modulation of Autophagy by Sorafenib: Effects on Treatment Response. Front Pharmacol. 2016; 7: 151.

6. Zhang X, Di C, Chen Y, Wang J, Su R, Huang G*, et al.* Multilevel regulation and molecular mechanism of poly (rC)-binding protein 1 in cancer. FASEB J. 2020; 34(12): 15647-15658.

7. Bradley RK, Anczukow O. RNA splicing dysregulation and the hallmarks of cancer. Nat Rev Cancer. 2023; 23(3): 135-155.

8. Tan CW, Sim DY, Zhen Y, Tian H, Koh J, Roca X. PRPF40A induces inclusion of exons in GC-rich regions important for human myeloid cell differentiation. Nucleic Acids Res. 2024; 52(15): 8800-8814.

9. Yang X, Yabe-Wada T, Han J, Saito F, Ogasawara C, Yamada S*, et al.* PCBP1 acts as a regulator of CCL2 expression in macrophages to induce recruitment of monocyte-derived macrophages into the inflamed colon. Int Immunol. 2023;

35(6): 287-299.

10. Nandal A, Ruiz JC, Subramanian P, Ghimire-Rijal S, Sinnamon RA, Stemmler TL*, et al.* Activation of the HIF prolyl hydroxylase by the iron chaperones PCBP1 and PCBP2. Cell Metab. 2011; 14(5): 647-657.

11. Zhang W, Shi H, Zhang M, Liu B, Mao S, Li L*, et al.* Poly C binding protein 1 represses autophagy through downregulation of LC3B to promote tumor cell apoptosis in starvation. Int J Biochem Cell Biol. 2016; 73: 127-136.

12. Ansa-Addo EA, Huang HC, Riesenberg B, Iamsawat S, Borucki D, Nelson MH*, et al.* RNA binding protein PCBP1 is an intracellular immune checkpoint for shaping T cell responses in cancer immunity. Sci Adv. 2020; 6(22): eaaz3865.

13. Ishii T, Hayakawa H, Igawa T, Sekiguchi T, Sekiguchi M. Specific binding of PCBP1 to heavily oxidized RNA to induce cell death. Proc Natl Acad Sci U S A. 2018; 115(26): 6715-6720.

14. Zhang Y, Meng L, Xiao L, Liu R, Li Z, Wang YL. The RNA-Binding Protein PCBP1 Functions as a Tumor Suppressor in Prostate Cancer by Inhibiting Mitogen Activated Protein Kinase 1. Cell Physiol Biochem. 2018; 48(4): 1747-1754.

15. Jiang P, Li Z, Tian F, Li X, Yang J. Fyn/heterogeneous nuclear ribonucleoprotein E1 signaling regulates pancreatic cancer metastasis by affecting the alternative splicing of integrin beta1. Int J Oncol. 2017; 51(1): 169-183.

16. Lee J, You JH, Roh JL. Poly(rC)-binding protein 1 represses ferritinophagy-mediated ferroptosis in head and neck cancer. Redox Biol. 2022; 51: 102276.

17. Protchenko O, Baratz E, Jadhav S, Li F, Shakoury-Elizeh M, Gavrilova O*, et al.* Iron Chaperone Poly rC Binding Protein 1 Protects Mouse Liver From Lipid Peroxidation and Steatosis. Hepatology. 2021; 73(3): 1176-1193.

18. Mariotto E, Viola G, Zanon C, Aveic S. A BAG's life: Every connection matters in cancer. Pharmacol Ther. 2020; 209: 107498.

19. Papadakis ES, Reeves T, Robson NH, Maishman T, Packham G, Cutress RI. BAG-1 as a biomarker in early breast cancer prognosis: a systematic review with meta-analyses. Br J Cancer. 2017; 116(12): 1585-1594.

20. Wu H, Liu M, He Y, Meng G, Guo W, Guo Q. Expression of BAG1 is associated with prognosis in kidney renal clear cell carcinoma based on bioinformatics. Bmc Cancer. 2021; 21(1): 160.

21. Rorke S, Murphy S, Khalifa M, Chernenko G, Tang SC. Prognostic significance of BAG-1 expression in nonsmall cell lung cancer. Int J Cancer. 2001; 95(5): 317-322.

22. Fan F, Yin R, Wang L, Zhao S, Lv D, Yang K*, et al.* ALDH3A1 driving tumor metastasis is mediated by p53/BAG1 in lung adenocarcinoma. J Cancer. 2021; 12(16): 4780-4790.

23. Bai YX, Yi JL, Li JF, Sui H. Clinicopathologic significance of BAG1 and TIMP3 expression in colon carcinoma. World J Gastroenterol. 2007; 13(28): 3883-3885.

24. D'Arcangelo D, Giampietri C, Muscio M, Scatozza F, Facchiano F, Facchiano A. WIPI1, BAG1, and PEX3 Autophagy-Related Genes Are Relevant

Melanoma Markers. Oxid Med Cell Longev. 2018; 2018: 1471682.

25. Ni W, Chen B, Zhou G, Lu C, Xiao M, Guan C*, et al.* Overexpressed nuclear BAG-1 in human hepatocellular carcinoma is associated with poor prognosis and resistance to doxorubicin. J Cell Biochem. 2013; 114(9): 2120-2130.

26. Kudoh M, Knee DA, Takayama S, Reed JC. Bag1 proteins regulate growth and survival of ZR-75-1 human breast cancer cells. Cancer Res. 2002; 62(6): 1904-1909.

27. Townsend PA, Cutress RI, Sharp A, Brimmell M, Packham G. BAG-1 prevents stress-induced long-term growth inhibition in breast cancer cells via a chaperone-dependent pathway. Cancer Res. 2003; 63(14): 4150-4157.

28. Kizilboga T, Baskale EA, Yildiz J, Akcay IM, Zemheri E, Can ND*, et al.* Bag-1 stimulates Bad phosphorylation through activation of Akt and Raf kinases to mediate cell survival in breast cancer. Bmc Cancer. 2019; 19(1): 1254.

29. Liu S, Ren B, Gao H, Liao S, Zhai YX, Li S*, et al.* Over-expression of BAG-1 in head and neck squamous cell carcinomas (HNSCC) is associated with cisplatin-resistance. J Transl Med. 2017; 15(1): 189.

30. Mariotto E, Corallo D, Pantile M, Giarin E, Pigazzi M, Basso G*, et al.* BAG1 down-regulation increases chemo-sensitivity of acute lymphoblastic leukaemia cells. J Cell Mol Med. 2021; 25(18): 9060-9065.

31. Pickering BM, Mitchell SA, Evans JR, Willis AE. Polypyrimidine tract binding protein and poly r(C) binding protein 1 interact with the BAG-1 IRES and stimulate its activity in vitro and in vivo. Nucleic Acids Res. 2003; 31(2): 639-

646.

32. Novak D, Huser L, Elton JJ, Umansky V, Altevogt P, Utikal J. SOX2 in development and cancer biology. Semin Cancer Biol. 2020; 67(Pt 1): 74-82.

33. Mirzaei S, Paskeh MDA, Entezari M, Mirmazloomi SR, Hassanpoor A, Aboutalebi M*, et al.* SOX2 function in cancers: Association with growth, invasion, stemness and therapy response. Biomed Pharmacother. 2022; 156: 113860.

34. Huser L, Novak D, Umansky V, Altevogt P, Utikal J. Targeting SOX2 in anticancer therapy. Expert Opin Ther Targets. 2018; 22(12): 983-991.

35. Liu B, Fang X, Kwong DL, Zhang Y, Verhoeft K, Gong L*, et al.* Targeting TROY-mediated P85a/AKT/TBX3 signaling attenuates tumor stemness and elevates treatment response in hepatocellular carcinoma. J Exp Clin Cancer Res. 2022; 41(1): 182.

36. Tang L, Wang D, Gu D. Knockdown of Sox2 Inhibits OS Cells Invasion and Migration via Modulating Wnt/beta-Catenin Signaling Pathway. Pathol Oncol Res. 2018; 24(4): 907-913.

37. Zhu Y, Huang S, Chen S, Chen J, Wang Z, Wang Y*, et al.* SOX2 promotes chemoresistance, cancer stem cells properties, and epithelial-mesenchymal transition by beta-catenin and Beclin1/autophagy signaling in colorectal cancer. Cell Death Dis. 2021; 12(5): 449.

38. Song P, Gao Z, Bao Y, Chen L, Huang Y, Liu Y*, et al.* Wnt/beta-catenin signaling pathway in carcinogenesis and cancer therapy. J Hematol Oncol. 2024; 17(1):

46.

39. Zhao Z, Cui T, Wei F, Zhou Z, Sun Y, Gao C*, et al.* Wnt/beta-Catenin signaling pathway in hepatocellular carcinoma: pathogenic role and therapeutic target. Front Oncol. 2024; 14: 1367364.

40. Leung HW, Leung CON, Lau EY, Chung KPS, Mok EH, Lei MML*, et al.* EPHB2 Activates beta-Catenin to Enhance Cancer Stem Cell Properties and Drive Sorafenib Resistance in Hepatocellular Carcinoma. Cancer Res. 2021; 81(12): 3229-3240.

41. Love MI, Huber W, Anders S. Moderated estimation of fold change and dispersion for RNA-seq data with DESeq2. Genome Biol. 2014; 15(12): 550.

42. Klopfenstein DV, Zhang L, Pedersen BS, Ramirez F, Warwick Vesztrocy A, Naldi A*, et al.* GOATOOLS: A Python library for Gene Ontology analyses. Sci Rep. 2018; 8(1): 10872.

43. Bu D, Luo H, Huo P, Wang Z, Zhang S, He Z*, et al.* KOBAS-i: intelligent prioritization and exploratory visualization of biological functions for gene enrichment analysis. Nucleic Acids Res. 2021; 49(W1): W317-W325.

44. Liu S, Huang F, Ru G, Wang Y, Zhang B, Chen X*, et al.* Mouse Models of Hepatocellular Carcinoma: Classification, Advancement, and Application. Front Oncol. 2022; 12: 902820.

45. Zheng Y, Zhou Z, Wei R, Xiao C, Zhang H, Fan T*, et al.* The RNA-binding protein PCBP1 represses lung adenocarcinoma progression by stabilizing DKK1 mRNA and subsequently downregulating beta-catenin. J Transl Med.

2022; 20(1): 343.

46. Hou M, Yue M, Han X, Sun T, Zhu Y, Li Z*, et al.* Comparative analysis of BAG1 and BAG2: Insights into their structures, functions and implications in disease pathogenesis. Int Immunopharmacol. 2024; 143(Pt 1): 113369.

47. Ma Z, Zhu P, Shi H, Guo L, Zhang Q, Chen Y*, et al.* PTC-bearing mRNA elicits a genetic compensation response via Upf3a and COMPASS components. Nature. 2019; 568(7751): 259-263.

48. Tripathi V, Sixt KM, Gao S, Xu X, Huang J, Weigert R*, et al.* Direct Regulation of Alternative Splicing by SMAD3 through PCBP1 Is Essential to the Tumor-Promoting Role of TGF-beta. Mol Cell. 2016; 64(5): 1010.

49. Guo C, Li S, Liu J, Ma Y, Liang A, Lou Y*, et al.* FBF1 maintains stem cell-like properties in breast cancer via PI3K/AKT/SOX2 axis. Stem Cell Res Ther. 2025; 16(1): 83.

50. Yang T, Zeng Y, Li Y, Huang Y, Meng X, Lu C*, et al.* Par6/SOX2 interact to modulate stemness maintenance in glioma by regulating the EGFR/PI3K/AKT signaling cascade. Oncogene. 2025; 44(46): 4441-4461.

51. Paz I, Argoetti A, Cohen N, Even N, Mandel-Gutfreund Y. RBPmap: A Tool for Mapping and Predicting the Binding Sites of RNA-Binding Proteins Considering the Motif Environment. Methods Mol Biol. 2022; 2404: 53-65.

52. Llovet JM, Kelley RK, Villanueva A, Singal AG, Pikarsky E, Roayaie S*, et al.* Hepatocellular carcinoma. Nat Rev Dis Primers. 2021; 7(1): 6.

53. Yu D, Hu H, Zhang Q, Wang C, Xu M, Xu H*, et al.* Acevaltrate as a novel

ferroptosis inducer with dual targets of PCBP1/2 and GPX4 in colorectal cancer. Signal Transduct Target Ther. 2025; 10(1): 211.

Ethics approval and consent to participate

This study includes patient-derived materials and the ethics approval or consent has been applied and approved [KY-XYZC-2024 (025)] by the Ethics Committee of Guangxi Branch of the First Affiliated Hospital of Sun Yat-sen University. Animal experiments were performed with approved from the Institutional Animal Care and Use Committee, Sun Yat-sen University (SYSU-IACUC-2024-002633). All research was conducted in accordance with both the Declarations of Helsinki. Written consent was given in writing by all subjects.

Data availability

All the data obtained and/or analyzed in the current study were available from the corresponding authors on reasonable request.

Conflict of Interest Statement

The authors declare no competing interests.

Funding

This work was supported in part by the Natural Science Foundation of China (No. 82573756; 82372656), the Natural Science Foundation of Guangdong Province (No.

2023A1515010415) to H. Wang, and Science and Technology Projects of Xizang Autonomous Region, China (XZ202502YD0002) from Xizang Minzu University.

Authors' contributions

Conception and design: H. Wang, Z. Li; Development of methodology: Z. Li, J. Yang; Acquisition of data (i.e., animals, molecular biology and cell biology experiments, facilities): Z. Li, J. Yang, C. Huang, J. Huang, Y. Fang, H. Qiu, Z. Hu, Q. Chen; Analysis and interpretation of data (e.g., statistical analysis, biostatistics, computational analysis): Z. Li, J. Yang, J. Huang, Z. Zhang, Y. Zhao; Writing the manuscript: H. Wang, Z. Li; Administrative, technical, or material support (i.e., reporting or organizing data, constructing databases): Z. Li, J. Yang, C. Huang, G. Lu, B. Xu; Study supervision: S. Yang, H. Wang. Approved manuscript: all authors.

Acknowledgments

We thank the professors Shijun Zhang for their technical assistance and valuable suggestions.

Supplemental information

Supplemental information including supplemental Figures S1-6 (PDF format) and supplemental Tables 1-4 (Docx format), respectively. Supplementary information is available at Molecular Medicine's website.

Supplementary Files

This is a list of supplementary files associated with this preprint. Click to download.

- SupplementaryFigures.docx
- SupplementaryTableS1.docx
- SupplementaryTableS2.docx
- SupplementaryTableS3.docx
- SupplementaryTableS4.docx
- OriginalData.pdf